

THESIS FOR THE DEGREE OF LICENTIATE OF ENGINEERING
in
Thermo and Fluid Dynamics

Extension of OpenFOAM Library for RANS Simulation of Premixed Turbulent Combustion

EHSAN YASARI

Department of Applied Mechanics
CHALMERS UNIVERSITY OF TECHNOLOGY
Göteborg, Sweden 2013

Extension of OpenFOAM Library for RANS Simulation of Premixed Turbulent Combustion

EHSAN YASARI

© EHSAN YASARI, 2013.

Thesis for Licentiate of Engineering no. 2013:10
ISSN 1652-8565

Department of Applied Mechanics
CHALMERS UNIVERSITY OF TECHNOLOGY
SE-412 96 Göteborg
Sweden
Telephone: +46(0)31- 772 1000

Typeset by the author using L^AT_EX.

Chalmers Reproservice
Göteborg, Sweden 2013

To my parents, Hosein & Fatemeh

Abstract

Unsteady multi-dimensional numerical simulation of turbulent flames is a well recognized tool for research and development of future internal combustion engines capable for satisfying stringent requirements for ultra-low emission and highly efficient energy conversion. To attain success, such simulations need, in particular, well elaborated Computational Fluid Dynamics (CFD) software, as well as advanced predictive models of turbulent burning.

As far as the software is concerned, a free, open source CFD software package called OpenFOAM (Open Field Operation And Manipulation) library has attracted increasing amounts of attention from both commercial and academic organizations over the past years. While the number of problems that have been studied using the package grows fast, applications of the code to Reynolds-Averaged Navier-Stokes (RANS) simulations of premixed turbulent flames are still rare and the standard version of OpenFOAM does not contain implementation of premixed turbulent combustion models with well documented predictive capabilities. Therefore, one goal of the present work was to further develop the code for multi-dimensional RANS simulations of premixed turbulent flames.

As far as models are concerned, a number of models of turbulent burning have been proposed to be used, but they strongly need straightforward quantitative testing against a wide and representative set of experimental data obtained in well defined simple cases under substantially different conditions. Therefore, another goal of the present work was to further validate two advanced models of the influence of turbulence on premixed combustion, i.e. the so-called Turbulent Flame Closure (TFC) and Flame Speed Closure (FSC) models.

The two models were implemented into OpenFOAM library and the so-extended code was successfully applied to simulate two widely recognized sets of experiments with two substantially different, well-defined, simple, laboratory premixed turbulent flames, i.e. (i) oblique, confined, preheated, highly turbulent, methane-air flames experimentally studied by Moreau [1] and (ii) V-shaped, open, weakly turbulent, lean methane-air flames investi-

ABSTRACT

gated by Dinkelacker and Hölzler [2] under the room conditions.

The obtained numerical results agree both qualitatively and quantitatively with the aforementioned experimental data, thus, validating both the implemented combustion models and the extended code. It is worth stressing that the influence of variations in the equivalence ratio on the measured data was quantitatively predicted without tuning. The ability of the TFC and FSC models and the extended code to accurately predict turbulent burning rates for various equivalence ratios make these two models and the associated code particularly attractive for use in multi-dimensional unsteady RANS simulations of turbulent combustion in Direct Injection Stratified Charge (DISC) Spark Ignition (SI) engines.

Keywords: Premixed turbulent combustion, TFC model, FSC model, Modeling, Simulation, Turbulent flow, OpenFOAM

List of publications

This thesis is based on the following three appended papers:

Paper 1

Ehsan Yasari, “Modification of the Temperature Calculation Library for Premixed Turbulent Combustion Simulation”, *6th OpenFOAM Conference*, June 2011, Pennsylvania, USA.

Paper 2

Ehsan Yasari, Andrei Lipatnikov, “Application of OpenFOAM Library to Simulation of Premixed Turbulent Combustion Using Flame Speed Closure Model”, *The 15th International Conference on Fluid Flow Technologies*, September 2012, Budapest, Hungary.

Paper 3

Ehsan Yasari, Andrei Lipatnikov, “RANS Simulations of Premixed Turbulent Flames Using TFC and FSC Combustion Models and OpenFOAM Library”, *The 6th European Combustion Meeting*, June 2013, Lund, Sweden.

Acknowledgments

First I want to thank Andrei Lipatnikov, my supervisor, who supports me through this project with his immense knowledge. I am really grateful for his help, guidance, and specially patience during this work and the time he spent for all explanations and discussions.

I also would like to thank Professor Ingemar Denbratt for giving me the opportunity to work as a PhD student in Combustion Division at Chalmers University of Technology.

Dr. Valeri Golovitchev is acknowledged for useful discussion and also helping me to work with CHEMKIN code. Thanks to Chen Huang and Anne Kösters for their time and help during the OpenFOAM code development and also for the CFD discussions we had together. A big thanks to Federico Ghirelli who help me to implement the TFC model in OpenFOAM and also gave me his implementations in OpenFOAM which make my work to be done faster. I am looking forward to continue our cooperation after my licentiate. I would like to thank Håkan Nilsson and Niklas Nordin for help with OpenFOAM. Professor Lars Davidson is acknowledged for teaching me a lot about turbulence modeling and turbulent flows.

The Swedish Energy Agency is acknowledged for the funding of this project and the CERC and Reference Group Meeting is acknowledged for useful discussions and meetings.

Thanks to all my colleagues in Combustion Division at Applied Mechanics, for the nice time having with them both inside and outside the Chalmers. Thanks to my office-mate Mirko Bovo for both scientific and non-scientific discussion we had, and also for his effort to help me to learn Swedish. Special thanks to Markus Grahn for his caring and also sharing this L^AT_EX template and supports for using it. Living in another country far from my family and friends was not easy specially in the beginning of my PhD, but I really would like to thank Gunnar Latz, Eugenio De Benito, Raúl Ochoterena, Lars Christian and Henrik Salsing who makes it much easier for me.

I also would like to thank all my Persian friends in Sweden specially Arash Eslamdoost who help me alot specially in the beginning of my stay

ACKNOWLEDGMENTS

in Gothenburg. I would like to highlight the “Fika/Lunch group” that I had enjoyable time being with them. Special thanks to two of my best friends in Iran, Saber Yekani Motlagh and Saeid Ganjeh Kaviri, for all their support and help which make me able to study abroad and also for all the enjoyable time we have together.

The last but not the least, I would like to thank my parents, Hosein and Fatemeh, and my sister Elham, for the love and support they gave me all these years. I would not be able to be here without them, and I cannot express how thankful I am that I have them.

Göteborg, May 2013

Nomenclature

Roman Symbols

a_{jk}	JANAF coefficients
A	a constant of TFC and FSC models
A', B'	coefficients in equation 2.42
b	combustion regress variable
c	combustion progress variable
C_D	coefficient to calculate length scale in k- ε model, see equation 2.39
C_μ	k- ε constant to calculate the turbulent viscosity, see equation 2.38
\tilde{C}_0	see equation 2.43
d	diameter
$Da = \tau_t/\tau_c$	Damköhler number
D_t	turbulent diffusivity
$D_{t,\infty}$	fully developed turbulent diffusivity
$D_{t,t}$	time dependent turbulent diffusivity
k	turbulent kinetic energy
L	turbulent length scale
L_E	Eulerian length scale
$L_{E,\perp}$	transversal Eulerian length scale
$L_{E,\parallel}$	longitudinal Eulerian length scale
L_L	Lagrangian length scale
M	molecular weight
p	pressure
P	probability density function
P_k	production term
$Pr_t = \nu_t/D_t$	turbulent Parndtl number
q	arbitrary quantity
Re	Reynolds number
Re_λ	Taylor microscale Reynolds number
S_{ij}	symmetric part of velocity gradient tensor
Sc	Schmidt number

NOMENCLATURE

Roman Symbols, continue

S_L	laminar flame speed
t	time
t_{fd}	flame development time
t_i	ignition time
t_r	reaction time scale
T	temperature
$u_i = u, v, w$	velocity components
u'	rms turbulent velocity
U_t	turbulent flame speed
$U_{t,\infty}$	full developed turbulent flame speed
W	reaction rate
$x_i = x, y, z$	spatial coordinates
X	arbitrary quantity
Y_k	mass fraction of the k -th specie

Greek Symbols

$\alpha(x, t)$	probability of finding fresh mixture
$\beta(x, t)$	probability of finding burned products
$\gamma(x, t)$	probability of finding burning mixture
δ	Dirac delta function
δ_t	turbulent flame brush thickness
ρ	Density
ε	dissipation rate
$\tau_t = L/u'$	turbulent time scale
$\tau_c = \kappa_u/S_L^2$	chemical time scale
$\tau_L = D_{t,\infty}/u'^2$	Lagrangian time scale
θ	activation temperature
κ	molecular heat diffusivity
ν	viscosity
$\sigma = \rho_u/\rho_b$	density ratio
$\sigma_k, \sigma_\varepsilon$	$k-\varepsilon$ model constant

Subscripts

b	burned
u	unburned
f	reacting mixture
r	reactant
p	product

Contents

Abstract	i
List of publications	iii
Acknowledgments	v
Nomenclature	vii
Contents	ix

I Introductory chapters

1 Introduction	1
2 Turbulent combustion modeling	5
2.1 Introduction	5
2.2 Introduction to the BML approach	5
2.3 Reynolds and Favre averaging	8
2.4 The governing equation	9
2.5 Overview of the TFC model	10
2.6 Overview of the FSC model	13
2.7 Turbulence model	14
2.8 Dissipation and Prandtl number tuning	15
3 Implementation of the models	19
3.1 Modification of the density calculation procedure in Open-FOAM	19
3.2 The implementation of the TFC and FSC models	23
4 Model validation	25
4.1 Introduction	25
4.2 Highly turbulent confined flames	26

CONTENTS

4.2.1	Simulated test case	26
4.2.2	Numerical setup	27
4.2.3	Results, validation, and discussion	29
4.2.4	Conclusion	47
4.3	V-shape flames	48
4.3.1	The simulated test case	48
4.3.2	Numerical setup and sensitivity analysis	48
4.3.3	Results, validation, and discussion	53
5	Concluding remarks and future work	65
References		67

II Included papers

Part I

Introductory chapters

Chapter 1

Introduction

Despite recent efforts to develop and exploit non-fossil sources of energy such as solar, wind and nuclear power, the combustion of fossil fuels still accounts for around 80% of the world's energy consumption. Fossil fuels are the dominant sources of energy in transport, heating, power production, and other important industries. The rapid rate at which fossil fuels are consumed and their finite reserves are significant causes for concern. However, the biggest problem arising from the global dependence on fossil fuels is that energy is not the only product of their combustion. In the ideal case, the complete combustion of a hydrocarbon-oxygen mixture produces water and CO_2 . This is troublesome because CO_2 is an important greenhouse gas, and the rising CO_2 emissions caused by fossil fuel combustion are a major driver of global climate change. Moreover, in real combustion systems, fossil fuels are not burned with perfect efficiency. Incomplete combustion yields harmful byproducts such as CO , NO_x , unburned hydrocarbons and soot. These chemical species pollute the air, threaten human health and contribute to global warming.

Because of these issues, legislation regarding the emission of pollutants from combustion processes has become increasingly stringent in recent years. The Kyoto protocol requires that various countries reduce their emissions of greenhouse gases such as CO_2 and water vapor. More specifically, vehicle manufacturers have been required to reduce the emissions generated by their products. In the European Union, the Euro 5 emission standards for all passenger cars have been in force since 2011. These regulations stipulate that passenger cars with gasoline engines must produce no more than 1 and 0.060 g/km of CO and NO_x , respectively. For diesel engines, the corresponding limits are 0.5 and 0.180 g/km , respectively. In addition, the regulations require that emissions of particulate matter (PM) must be below 0.005 g/km for both engine types. Even stricter limits will be imposed in 2014, when the Euro 6 standards will come into force. These standards

CHAPTER 1. INTRODUCTION

will require that NO_x emissions be reduced to 0.080 and 0.060 g/km for diesel and gasoline engines, respectively. Different sets of limitations will be applied for light commercial vehicles and trucks.

One of the most important ways for manufacturers to satisfy these demanding requirements is to further optimize the combustion process. This requires a detailed understanding of the combustion process and its sensitivity to turbulence. Such understanding can only be acquired via a combination of advanced experimental investigations and unsteady multi-dimensional simulations. Experiments are very important sources of real-world data. However, they are usually expensive to perform and can only provide limited information on certain aspects of the physical processes involved in combustion. Simulations using Computational Fluid Dynamic(CFD) are powerful tools that are comparatively inexpensive to perform and which can provide useful data that is often complementary to experimental results. Importantly, CFD simulations can be used to study a range of physical phenomena that may be inaccessible using conventional experimental techniques. They are therefore useful tools for predicting the performance of new designs prior to the production of prototypes. However, it is essential to carefully validate the performance of CFD models by comparing their output to experimental data.

Although several mature commercial CFD codes have been developed and are widely used, there is a strong demand for less expensive software within the commercial sector. Moreover, academics are very interested in having access to the source code of the programs they use since this enables them to develop and implement new models and to easily exchange information and data. For these reasons, the Open Field Operation and Manipulation (OpenFOAM) library - a free, open source CFD software package that is available at www.openfoam.com - has attracted increasing amounts of attention from both commercial and academic organizations since its first release in 2004. However, although the number of problems relevant to internal combustion engines that have been studied with OpenFOAM continues to grow, there are still many such problems that have not yet been addressed with this code. Consequently, many more studies will be required in order to properly assess its utility in the automotive and gas turbine industry.

Accordingly, **first goal** of the present work is to assess the potential of this code (and to develop it further if necessary) as a tool for conducting multi-dimensional Reynolds- Averaged Navier-Stokes (RANS) simulations of premixed turbulent combustion.

In addition to an efficient CFD code, a predictive model that can describe the influence of turbulence on premixed flames is required in order

to investigate burning in devices such as Spark Ignition (SI) reciprocating engines, Lean Premixed Prevaporized (LPP) gas turbine combustors, and aero-engine afterburners.

Although a number of premixed turbulent combustion models are available, the vast majority of them have not been validated in a straightforward way against a wide range of targets. For example, certain models were recently tested by quantitatively comparing expressions for turbulent flame speed derived from those models in the planar, one-dimensional, stationary case to the measured speeds of curved and developing laboratory flames (i.e. expanding spherical flames). However, tests of this kind cannot be considered to provide straightforward validation of a model's performance and reliability because empirical measurements of the turbulent flame speed are well known to depend heavily on the method of measurement used.

Of the various models that can be used in RANS simulations of premixed turbulent combustion, only two classes have been used to simulate a broad range of laboratory flame types in a straightforward way. These are (i) the Eddy-Break-Up model of Spalding [3] and the related model proposed by Magnussen and Hjertager [4], and (ii) the so-called Turbulent Flame Closure (TFC) model of Zimont and Lipatnikov [5]. Studies on the models of the first class revealed that it was necessary to adjust the values of key model parameters on a case-by-case basis in order to reproduce experimental results for different flame types. In contrast, the TFC model yielded results that closely matched the available experimental data for a broad range of flame types without requiring such case-by-case parameter tuning.

Lipatnikov and Chomiak [6] extended the TFC model in order to (i) simulate weakly turbulent combustion, (ii) describe the early stages of flame development, and (iii) facilitate the establishment of boundary conditions. Their expanded TFC model was named the Flame Speed Closure (FSC) model and has since been validated against experimental data reported by various research groups on a wide range of expanding, statistically spherical, premixed turbulent flames [6]. Therefore, the **second goal** of this project was to implement the TFC and FSC models in OpenFOAM.

The **third goal** of this project was to validate the implemented combustion models against different sets of experimental data. Due to the complexity of combustion in engines, which involves not only burning itself, but also injection, evaporation, turbulent mixing, heat losses, etc., and due to the general shortcomings of the available experimental data (which in many cases consist exclusively of pressure curves), there is generally considerable scope for the tuning of key model parameters when testing models of turbulent combustion for use in engine simulations. While such tests are necessary, they only seem to be valuable once the models in question have

CHAPTER 1. INTRODUCTION

been extensively validated against a wide-ranging set of experimental data for well-defined simple cases. A validation exercise of this sort is presented herein.

In this work, the TFC and FSC models were tested against two sets of experimental data for statistically stationary flames. The decision to focus on stationary flames was motivated by two key considerations. First, the project presented herein was a component of a larger project whose aim is to develop models that can be used to address the counter-gradient problem. However, the only available experimental data that can be used to validate such models relate to stationary flames, because it would be prohibitively expensive to conduct appropriate experiments on expanding flames. Moreover, before this work was undertaken, the FSC model had only been validated against a single statistically stationary premixed turbulent flame - specifically, an oblique confined flame stabilized behind a bluff body [7]. It was therefore considered important to validate this model against a more extensive set of experimental data for statistically stationary premixed turbulent flames. The **fourth goal** of this work was thus to determine whether or not the extensions that differentiate the FSC and TFC models are important for describing the behavior of stationary flames.

Chapter 2

Turbulent combustion modeling

2.1 Introduction

This chapter begins with a summary of the BML approach, after which Reynolds and Favre averaging are introduced. The third section presents the governing equations. Two combustion models are introduced, followed by the $k-\varepsilon$ turbulence model, in sections 2.5, 2.6 and 2.7, respectively. The final section discusses problems arising from uncertainties associated with the boundary values of the dissipation rate and Prandtl number in numerical simulations.

2.2 Introduction to the BML approach

The BML model was introduced in 1977 by Bray, Moss, and Libby [8] [9], and is named for its authors. This section provides a brief overview of the model's underlying principles. It was developed based on the assumption that $Re \gg Da \gg 1$, where Da is the Damköhler number and is defined as the ratio of the turbulent time scale, τ_t , to the chemical time scale, τ_c . In most combustion processes, the latter is much shorter than the former and so Da is usually large. Moreover, the reaction zone is assumed to be infinitely small. Consequently, the mean flame brush thickness can be described in terms of an ensemble average of the thin flame surface.

In general the probability density function(PDF) of finding arbitrary value of q at a given location and time, (x, t) , is

$$P(x, t, q) = \alpha(x, t)P_u(x, t) + \beta(x, t)P_b(x, t) + \gamma(x, t)P_f(x, t, q), \quad (2.1)$$

where $\alpha(x, t)$, $\beta(x, t)$, $\gamma(x, t)$ are the probabilities of finding the fresh mixture, burned product and burning mixture, respectively. The subscripts

u , b and f correspond to the fresh mixture, burned products and reacting mixture, respectively. Two such PDFs are shown in figure 2.1(a).

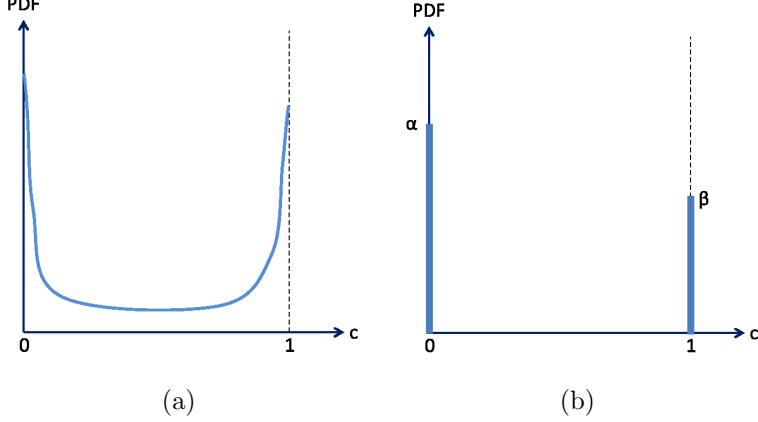


Figure 2.1: PDFs for a) the flamelet regime b) the bi-modal approximation used in the BML approach

The BML model uses a presumed PDF of the progress variable c , which denotes the state of the mixture ($c=0$ for fresh mixture and $c=1$ for burned products) at a given location and time (x, t)

$$P(x, t, c) = \alpha(x, t)\delta(c) + \beta(x, t)\delta(1 - c) + \gamma(x, t)P_f(x, t, c), \quad (2.2)$$

where $\delta(c)$ and $\delta(1 - c)$ are the Dirac delta functions correspond to fresh mixture and burned products, respectively. Comparing to equation 2.1 one can say

$$P_u(x, t) = \delta(c) \quad P_b(x, t) = \delta(1 - c). \quad (2.3)$$

In general, equation 2.2 is not suitable for practical use because both the LHS and the RHS feature unknown PDF functions, $P(x, t, c)$ and $P_f(x, t, c)$. However in the case where $\gamma(x, t) \ll 1$ within the flame brush and with the following properties of PDF and Dirac delta function

$$\int_{-\infty}^{\infty} f(x)\delta(x - a)dx = f(a) \quad \int_{-\infty}^{\infty} P(x)dx = 1, \quad (2.4)$$

where $f(x)$ is an arbitrary continuous function at $x = a$, one can write

$$\alpha(x, t) + \beta(x, t) = 1, \quad (2.5)$$

$$P(x, t, c) \approx \alpha(x, t)\delta(c) + \beta(x, t)\delta(1 - c). \quad (2.6)$$

The assumption of $\gamma(x, t) \ll 1$ means that one can replace the real PDF in equation 2.2, which is shown in figure 2.1(a), with the so-called

2.2. INTRODUCTION TO THE BML APPROACH

bi-modal PDF, equation 2.6. The bi-modal PDF consists of two Dirac delta functions at $c=0$ and $c=1$ and is shown in figure 2.1(b). $\alpha(x, t)$ and $\beta(x, t)$ in equation 2.6 are unknown, and so the objective becomes to determine the values of these parameters.

For any arbitrary function $f(c)$

$$\overline{f(c)} = \int_{-\infty}^{\infty} f(c)P(x, t, c)dc, \quad (2.7)$$

One can therefore derive the following based on the properties of the PDF and the Dirac functions used in equation 2.4

$$\begin{aligned} \bar{c}(x, t) &= \int_{-\infty}^{\infty} c(x, t)P(x, t, c)dc \\ &= \int_0^1 c(x, t)[\alpha(x, t)\delta(c) + \beta(x, t)\delta(1 - c)]dc \\ &= \alpha(x, t)c(x, t)_{c=0} + \beta(x, t)c(x, t)_{c=1} \\ &= \beta(x, t), \end{aligned} \quad (2.8)$$

This shows that \bar{c} is equal to the probability of finding burned products, and therefore

$$\alpha = 1 - \bar{c}(x, t). \quad (2.9)$$

For the sake of simplicity, $c(x, t)$, $P(x, t, c)$, $\alpha(x, t)$ and $\beta(x, t)$ are replaced by c , $P(c)$, α and β in the following discussion.

In general, for an arbitrary quantity, X , one can write

$$\bar{X} = \alpha X_u + \beta X_b = (1 - \bar{c})X_u + \bar{c}X_b, \quad (2.10)$$

$$\overline{\rho c} = \tilde{\rho} \bar{c} = \int_0^1 \rho c P(c)dc = \alpha \cdot (\rho c)_{c=0} + \beta \cdot (\rho c)_{c=1} = \rho_b \beta, \quad (2.11)$$

and

$$\begin{aligned} \bar{\rho} &= \int_0^1 \rho P(c)dc = \alpha \cdot (\rho)_{c=0} + \beta \cdot (\rho c)_{c=1} \\ &= \alpha \rho_u + \beta \rho_b \\ &= (1 - \bar{c})\rho_u + \bar{c}\rho_b. \end{aligned} \quad (2.12)$$

where the overbar and overtilde represent the Reynolds and Favre averages, respectively. The relevance of these quantities is discussed in the following section.

2.3 Reynolds and Favre averaging

This section introduces Reynolds and Favre averaging, and explains Favre averaging is preferred to the more common Reynolds average in combustion simulations. Reynolds averaging is widely used to analyze non-reacting flows, where there are no fluctuations in flow density. Based on the definition of the Reynolds average, an arbitrary quantity such as X can be split into a mean value \bar{X} and a deviation from the mean, X'

$$X = \bar{X} + X', \quad \bar{X}' = 0 \quad (2.13)$$

and for a statistically stationary process, \bar{X} is defined as

$$\bar{X} = \frac{1}{\Delta t} \int_0^{\Delta t} X dt, \quad (2.14)$$

where Δt is a time interval. This type of averaging can be applied to the instantaneous balance equations, giving the Reynolds Averaged Naiver-Stokes(RANS) equations.

However in reacting flows, heat release causes fluctuations in density and therefore Reynolds averaging produces an extra un-closed term. Indeed

$$\begin{aligned} \frac{\partial \bar{\rho}}{\partial t} + \frac{\partial \bar{\rho} u_j}{\partial x_j} &= 0 \Rightarrow \frac{\partial \bar{\rho}}{\partial t} + \frac{\partial (\bar{\rho} + \rho')(\bar{u}_j + u'_j)}{\partial x_j} = 0 \Rightarrow \\ \frac{\partial \bar{\rho}}{\partial t} + \frac{\partial \bar{\rho} \bar{u}_j + \bar{\rho}' u'_j}{\partial x_j} &= 0, \end{aligned} \quad (2.15)$$

where the overlines denote the Reynolds averages and $\bar{\rho}' u'_j$ is an unknown term that can only be closed by modeling. These unclosed terms can be avoided by using Favre averaging instead

$$\tilde{X} = \frac{\bar{\rho} \bar{X}}{\bar{\rho}}, \quad (2.16)$$

where $\bar{\rho}$ is the Reynolds average density and the tilde denotes Favre averaging. From the above, it follows that

$$X = \tilde{X} + X'', \quad \tilde{X}'' = 0, \quad \bar{X}'' \neq 0. \quad (2.17)$$

No extra unknown terms are created when the instantaneous mass conservation equation is subjected to Favre averaging. Indeed

$$\frac{\partial \bar{\rho}}{\partial t} + \frac{\partial \bar{\rho} u_j}{\partial x_j} = 0 \Rightarrow \frac{\partial \bar{\rho}}{\partial t} + \frac{\partial \bar{\rho} \tilde{u}_j}{\partial x_j} = 0. \quad (2.18)$$

2.4. THE GOVERNING EQUATION

Therefore, for all transport equations that are commonly used in combustion simulations, Favre averaging is used in preference to Reynolds averaging. The next section presents some of the Favre-averaged balance equations used in this work.

By applying the definition of the Favre average and combining equations 2.8, 2.9, 2.11 and 2.12, one obtains the following

$$\bar{\rho} = \frac{\rho_u}{1 + (\sigma - 1)\tilde{c}}, \quad (2.19)$$

where $\sigma = \rho_u/\rho_b$ is the density ratio

$$\bar{c} = \frac{\sigma\tilde{c}}{1 + (\sigma - 1)\tilde{c}}. \quad (2.20)$$

Equation 2.20 is used to convert Favre-averaged progress values into their Reynolds-averaged equivalents.

2.4 The governing equation

As discussed in the previous section, Favre averaging is generally used in combustion simulations where the density of the reacting flow fluctuates significantly. This section presents the Favre-averaged balance equations for mass, momentum, and the progress variable.

- Mass:

$$\frac{\partial \bar{\rho}}{\partial t} + \frac{\partial \bar{\rho}\tilde{u}_j}{\partial x_j} = 0, \quad (2.21)$$

- Momentum:

$$\frac{\partial \bar{\rho}\tilde{u}_i}{\partial t} + \frac{\partial \bar{\rho}\tilde{u}_j\tilde{u}_i}{\partial x_j} = -\frac{\partial \bar{p}}{\partial x_i} + \mu \frac{\partial^2 \tilde{u}_j}{\partial x_j \partial x_i} - \frac{\partial \tau_{ij}}{\partial x_j}, \quad (2.22)$$

where $\tau_{ij} = \bar{\rho}\tilde{u}_j''\tilde{u}_i''$ is the Reynolds stresses tensor.

- Progress variable:

$$\frac{\partial \bar{\rho}\tilde{c}}{\partial t} + \frac{\partial(\bar{\rho}\tilde{u}_j\tilde{c})}{\partial x_j} = -\frac{\partial}{\partial x_j}(\overline{\rho u_j'' c''}) + \bar{\rho}\tilde{W}. \quad (2.23)$$

In these equations, t is time while x_j and \tilde{u}_j are the coordinate and velocity components, respectively. $\bar{\rho}$ is the mean density; in the BML framework, this is computed using equation 2.19. \bar{p} and μ are the pressure and dynamic viscosity, respectively, and c is the progress variable (where a value of $c=0$

corresponds to the unburned mixture and $c=1$ corresponds to the completely burned product) that is used to characterize the state of the mixture (assuming that it is undergoing premixed adiabatic turbulent combustion). The first and second terms on the RHS of equation 2.23 represent the turbulent heat flux and the mean reaction rate, respectively. This equation is discussed in more detail in the next section.

The goal in turbulence and combustion modeling is to close the unknown terms in the equations discussed above. Different turbulence models and combustion models use different expressions for this purpose.

Different models have been developed to close the transport equation for the progress variable, i.e. equation 2.23. The simplicity of Eddy Break Up(EBU) model of Spalding [3] makes it quite attractive in three dimensional engine simulations and therefore available in most commercial CFD codes. Reaction rate in this model is based on the known quantities such as the turbulent mixing timescale, which is assumed to equal the ratio of the turbulent kinetic energy to the rate of dissipation. Consequently, it does not require an extra transport equation. However, it cannot predict how the mixture's composition and chemical characteristics will affect the turbulent burning rate, and manual adjustment of the model's constants is required to obtain useful results for different fuels and operating conditions.

More sophisticated combustion models that can describe premixed turbulent combustion have been developed in recent years. One such approach, which is believed to have considerable potential for use in three dimensional combustion simulations, involves computing the turbulent burning rate in order to close the balance equation for the progress variable. Two of the more widely used models of this type are presented in sections 2.5 and 2.6.

Turbulence models can also be used to obtain approximate estimates of the Reynolds stresses, $\widetilde{u_j''u_i''}$. This finding led to the development of the $k - \varepsilon$ model, which is based on eddy viscosity model and the Boussinesq assumption and is discussed further in section 2.7.

2.5 Overview of the TFC model

The TFC model relies on a single transport equation (equation 2.23) to compute the progress variable that is used to characterize the state of the mixture under the assumption of a premixed, adiabatic turbulent combustion process.

As mentioned above, the main difficulty associated with using this equation to simulate premixed turbulent combustion is that one must somehow close the unknown terms on the RHS of the equation. Two different solutions to this problem have been developed. One is supposedly based on first

2.5. OVERVIEW OF THE TFC MODEL

principles while the other is more phenomenological.

While the first approach appears to have a more fundamental basis, the resulting expressions typically contain many unknown terms that must be closed by modeling. In addition, this approach often necessitates the inclusion of some constant whose universality is questionable, meaning that there is considerable scope for tuning. This approach will therefore require further development before it will be ready for practical use.

The second approach uses well-established experimental phenomena to close the RHS of equation 2.23. Equation 2.24 was proposed by Zimont and Lipatnikov [5] based on the pioneering work of Prudnikov [10], [11] regarding the growth of the mean flame brush thickness δ_t in a typical premixed turbulent flame.

$$\frac{\partial \bar{c}}{\partial t} + \frac{\partial(\bar{\rho}\tilde{u}_j\tilde{c})}{\partial x_j} = \frac{\partial}{\partial x_j} \left(\bar{\rho}D_t \frac{\partial \tilde{c}}{\partial x_j} \right) + \rho_u U_t |\nabla \tilde{c}| \quad (2.24)$$

Here, D_t is the turbulent diffusivity. In the framework of k- ε model, it is defined as

$$D_t = D_{t,\infty} = \frac{C_\mu}{Pr_t} \frac{\tilde{k}^2}{\tilde{\varepsilon}} \quad (2.25)$$

According to this method, the mean flame brush thickness behavior and turbulent burning rate are controlled by the first and second terms on the RHS of equation 2.24.

A submodel for turbulent flame speed is also required. Zimont [12] introduced the following submodel for this purpose

$$U_{t,\infty} = Au' Da^{1/4} = Au' \left[\frac{\tau_t}{\tau_c} \right]^{1/4} = Au' \left[\frac{L/u'}{\kappa_u/S_L^2} \right]^{1/4} \quad (2.26)$$

It should be noted that local processes occurring in turbulent flames are not explicitly accounted for in equation 2.24. However, the effects of such processes on the mean rate of heat release are accounted for using a submodel for the turbulent burning rate that is defined by equation 2.26.

Here, A is a constant associated with the model. Da is the Damköhler number and is defined as $Da = \frac{\tau_t}{\tau_c}$, where $\tau_t = \frac{L}{u'}$ and $\tau_c = \frac{\kappa_u}{S_L^2}$ are the turbulent and chemical time scales, respectively. u' , κ_u and S_L are the fluctuation in the turbulent velocity, the molecular heat diffusivity for the unburned material, and the laminar flame speed, respectively.

One of the main features of this model is that it describes the effects of the mixture's composition on the turbulent burning rate in terms of a single variable: the chemical time scale, τ_c . Moreover, it only features one

CHAPTER 2. TURBULENT COMBUSTION MODELING

constant, making it a simple predictive tool that is quite straightforward to use in three dimensional simulations of premixed combustion processes.

An additional major strength of this approach is that a number of empirical trends derived from measurements of turbulent flame speed and burning velocity, such as the tendency for U_t and the laminar flame speed to increase during turbulent velocity fluctuations, are accurately reproduced in simulations conducted using equation 2.26.

Equations 2.24 and 2.26 together comprise the Turbulent Flame Closure (TFC) model, which was derived by considering the intermediate transient regime that is characterized by a gradual increase in flame brush thickness with a constant turbulent burning velocity.

It is also worth noting that in the framework of the TFC model, the sum of the terms on the RHS of equation 2.23 is equal to that of the terms on the RHS of equation 2.24. In other words, equation 2.24 is a global model for equation 2.23 and so one can say that

$$-\frac{\partial}{\partial x_j}(\bar{\rho}u''_j c'') + \bar{\rho}\tilde{W} = \frac{\partial}{\partial x_j}\left(\bar{\rho}D_t \frac{\partial \tilde{c}}{\partial x_j}\right) + \rho_u U_t |\nabla \tilde{c}|. \quad (2.27)$$

As such, this method does not prescribe specific approaches for modeling the individual terms. Submodels for evaluating the turbulent flux in equation 2.27 [13], [14], [15] and [16] are beyond the scope of the present work.

The TFC model has been validated by multiple research groups in various experiments that have been reviewed elsewhere [6].

Overall, the results obtained to date show that the TFC model is a promising tool for use in three dimensional simulations of premixed turbulent combustion. However, it has some noteworthy limitations that will need to be addressed in order to make it more practically useful specially in SI engine simulations.

First, the laminar burning velocity can be significant at high temperatures and pressures such as those that occur in SI engines. However, the TFC model was developed to describe situations involving moderate turbulence, i.e. cases where $u' > S_L$, and predicts a burning velocity of zero when the turbulence intensity is low (specifically, when $u' \rightarrow 0$).

Second, the TFC model describes the burning velocity of the developed flame and so cannot describe the early stages of flame development. The transition from laminar to turbulent burning is an important component of combustion in SI engines and in some laboratory combustion situations (e.g. bombs). Consequently, there is a need for models that can describe this stage of the combustion process as well.

Third, in cases where the Neumann boundary condition applies at all of

2.6. OVERVIEW OF THE FSC MODEL

the system's boundaries, any $\tilde{c} = \text{const}$ can be a solution of equation 2.24.

These limitations are addressed in the FSC model, which is discussed in 2.6.

2.6 Overview of the FSC model

As discussed in section 2.5, the TFC model has some limitations and required further development to make it generally applicable in three dimensional combustion simulations. This prompted the creation of the FSC model [17] [18] [6], which addresses some of the deficiencies of its predecessor. Notably, the equations for the turbulent diffusivity and turbulent flame speed from the TFC model were modified to allow the model to describe the early stages of flame development, yielding equations 2.28 and 2.29, respectively.

$$D_{t,t} = D_{t,\infty} \left[1 - \exp \left(-\frac{t_{fd}}{\tau_L} \right) \right], \quad (2.28)$$

$$U_{t,t} = U_{t,\infty} \left\{ 1 + \frac{\tau_L}{t_{fd}} \left[\exp \left(-\frac{t_{fd}}{\tau_L} \right) - 1 \right] \right\}^{1/2}, \quad (2.29)$$

The fully developed quantities $D_{t,\infty}$ and $U_{t,\infty}$ are defined in equations 2.25 and 2.26, respectively. $\tau_L = D_{t,\infty}/u'^2$ and the flame development time $t_{fd} = t - t_i$ are counted relative to the time of ignition, t_i . However, in the case of stationary flames, t_{fd} can be replaced by the ratio of the distance from flame holder, x , to the mean gas flow velocity, u_1 .

Another difference between the TFC and FSC models is that the latter appends a laminar-like source term derived from laminar flame theory to equation 2.24, enabling the FSC model to overcome the first and third limitations of the TFC model. The modified term has the following form

$$\begin{aligned} \frac{\partial \bar{\rho} \tilde{c}}{\partial t} + \frac{\partial (\bar{\rho} \tilde{u}_j \tilde{c})}{\partial x_j} &= \frac{\partial}{\partial x_j} \left[\bar{\rho} (D_{t,t} + \kappa) \frac{\partial \tilde{c}}{\partial x_j} \right] \\ &+ \frac{\bar{\rho} (1 - \tilde{c})}{t_r (1 + D_{t,t}/\kappa_b)} \exp \left(-\frac{\theta}{\bar{T}} \right) \\ &+ \rho_u U_{t,t} |\nabla \tilde{c}|, \end{aligned} \quad (2.30)$$

Here, κ is the laminar diffusivity, θ is the activation temperature for a single reaction model, and t_r is the time scale, which is assigned a value such that equation 2.30 yields the known value of S_L in the case of planar steady flame propagation at $u' = 0$. The Favre-averaged temperature is calculated using the Favre-averaged progress variable as follows

$$\tilde{T} = T_u \cdot (1 - \tilde{c} + \sigma \tilde{c}), \quad (2.31)$$

where $\sigma = \rho_u / \rho_b$ is the density ratio. It is clear that equation 2.30 can predict the laminar burning velocity in the limit case of $u' = D_{t,t} = U_{t,t} = 0$ because under such conditions it reduces to the balance equation of the laminar flame theory [19].

The FSC model [17] [18] [6] consists of equations 2.30 (with and without the exponential source term), 2.28 and 2.29. Notably, it overcomes the limitations of the TFC model without introducing any new constants.

2.7 Turbulence model

The transport equation for the kinetic energy in the standard $k-\varepsilon$ model is as follows,

$$\frac{\partial \bar{\rho} \tilde{k}}{\partial t} + \tilde{u}_j \frac{\partial \bar{\rho} \tilde{k}}{\partial x_j} = \bar{\rho} P_k - \bar{\rho} \tilde{\varepsilon} + D_t^k. \quad (2.32)$$

The first and second terms on the LHS describe the variation of the kinetic energy over time and due to convection, respectively. P_k is the production term and must be computed by modeling due to the presence of the Reynolds stress tensor, which is unknown. In the linear eddy viscosity model, Reynolds stresses are modeled using the Boussinesq assumption, yielding the following expression for P_k

$$P_k = -\widetilde{u'_i u'_j} \frac{\partial \tilde{u}_i}{\partial x_j} = \nu_t \left(\frac{\partial \tilde{u}_i}{\partial x_j} + \frac{\partial \tilde{u}_j}{\partial x_i} \right) \frac{\partial \tilde{u}_i}{\partial x_j} = 2\nu_t \widetilde{S}_{ij} \widetilde{S}_{ij}, \quad (2.33)$$

where \widetilde{S}_{ij} is the symmetric part of the velocity gradient tensor and is defined as follows

$$\widetilde{S}_{ij} = \frac{1}{2} \left(\frac{\partial \tilde{u}_i}{\partial x_j} + \frac{\partial \tilde{u}_j}{\partial x_i} \right). \quad (2.34)$$

The second term on the RHS of the k equation is the *dissipation* term; its value is obtained from the dissipation term of the transport equation (i.e. equation 2.36).

D_t^k in equation 2.32 is the turbulent diffusion term and must be modeled. Based on the gradient hypothesis, this term can be modeled using equation 2.35.

$$D_t^k = -\frac{\partial}{\partial x_j} \left(\bar{\rho} \frac{\nu_t}{\sigma_k} \frac{\partial \tilde{k}}{\partial x_j} \right). \quad (2.35)$$

2.8. DISSIPATION AND PRANDTL NUMBER TUNING

The modeled dissipation transport equation reads

$$\frac{\partial \bar{\rho} \tilde{\varepsilon}}{\partial t} + \tilde{u}_j \frac{\partial \bar{\rho} \tilde{\varepsilon}}{\partial x_j} = \bar{\rho} \frac{\tilde{\varepsilon}}{\tilde{k}} (c_{\varepsilon 1} P_k - c_{\varepsilon 2} \tilde{\varepsilon}) + \frac{\partial}{\partial x_j} \left[\bar{\rho} \frac{\nu_t}{\sigma_{\varepsilon}} \frac{\partial \tilde{\varepsilon}}{\partial x_j} \right] - c_{\varepsilon 3} \bar{\rho} \tilde{\varepsilon} \frac{\partial \tilde{u}_i}{\partial x_i}. \quad (2.36)$$

The constants used in the k- ε model are as follows

$$\sigma_k = 1 \quad \sigma_{\varepsilon} = 1.3 \quad c_{\varepsilon 1} = 1.44 \quad c_{\varepsilon 2} = 1.92 \quad c_{\varepsilon 3} = -0.33 \quad (2.37)$$

In the standard k- ε model, $c_{\varepsilon 3} = 0$.

The ν_t term in the k equation represents the turbulent viscosity and is defined as

$$\nu_t = c_{\mu} \frac{\tilde{k}^2}{\tilde{\varepsilon}} \quad (2.38)$$

where the constant c_{μ} is equal to 0.09.

All of the transport equations used in this work have been presented and discussed in this section and the two that preceded it. The following section provides a brief overview of the algorithm used to solve these equations. The balance equations for velocity and pressure are solved using an iterative algorithm of the type used in the incompressible case. However, because the density is not constant, it is calculated using equation 2.19 and the values of \tilde{c} are obtained by solving equation 2.24. The basic procedure is as follows:

- Solving the velocity equation with an initial guess for pressure
- Solve for the progress variable by using the velocity field obtained from previous step and calculating the density of the reacting mixture
- Solve the Poisson equation for pressure using the velocity field obtained in the previous step
- Correct the velocity field with the new pressure field
- Repeat the steps above until the solution converges

2.8 Dissipation and Prandtl number tuning

As mentioned in the previous sections, there is in principle only one constant (A) to be tuned in both the TFC and FSC models. However, some additional tuning may be required even if A is held constant. In order to evaluate the predicted flow fields generated using combustion models, it is necessary

CHAPTER 2. TURBULENT COMBUSTION MODELING

to perform some modeling using turbulence models. This introduces two notable sources of uncertainty when dealing with RANS simulations. The first relates to the rate of dissipation at the boundary while the second is associated with the turbulent Prandtl number, Pr_t . This section discusses these uncertainties and describes methods for addressing them that have been proposed by different research groups.

To simulate a turbulent flow using the $k-\varepsilon$ model, one must know the value of $\bar{\varepsilon}$ at the inlet boundary. However this value is not generally reported in experimental papers; at best, a value for the length scale will be reported but not defined. If the value of the length scale is known, the dissipation rate can be calculated using equation 2.39, where L is the integral length scale.

$$\bar{\varepsilon} = \frac{C_D \tilde{k}^{3/2}}{L} \quad (2.39)$$

However, it is not clear what integral length scale should be substituted in this equation, and different length scales yield substantially different results. For example, according to Shchetnikov [20], in a fully developed turbulent flow in a tube,

$$L_L = 0.02d \quad ; \quad L_E = 0.04d \quad (2.40)$$

where L_L and L_E are the Lagrangian and Eulerian length scales, respectively, and d is the tube diameter. However it is not clear whether it is the longitudinal, $L_{E,\parallel}$, or transversal, $L_{E,\perp}$, Eulerian length scale that is meant here.

In homogeneous isotropic turbulence, $L_{E,\parallel} = 2L_{E,\perp}$. Therefore, the length scale in equation 2.39 cannot be greater than $0.08d$ if $L_{E,\perp} = 2L_L$, i.e. $L_{E,\parallel}/L_L < 8$. However, Brodkey found that the inverse of this ratio can range from 2 to 6.5. [21]

These uncertainties regarding the length scale introduce uncertainty into the value of the constant used in equation 2.39. For example, Pope [22] suggested the following equation

$$\bar{\varepsilon} = 0.43 \frac{\bar{k}^{3/2}}{L_{E,\parallel}} \approx 0.77 \frac{u'^3}{L_{E,\parallel}} \quad (2.41)$$

However, Dahms et al. [23] invoked $\bar{\varepsilon} = 0.37 \frac{u'^3}{L}$.

Moreover, DNS data analyzed by Sreenivasan [24] indicate that C_D depends on the nature of the forcing applied at low wave numbers and on the Re number, as shown in figure 2.2. In this case, C_D increases rapidly when the Taylor microscale Reynolds number, Re_λ , is decreased.

2.8. DISSIPATION AND PRANDTL NUMBER TUNING

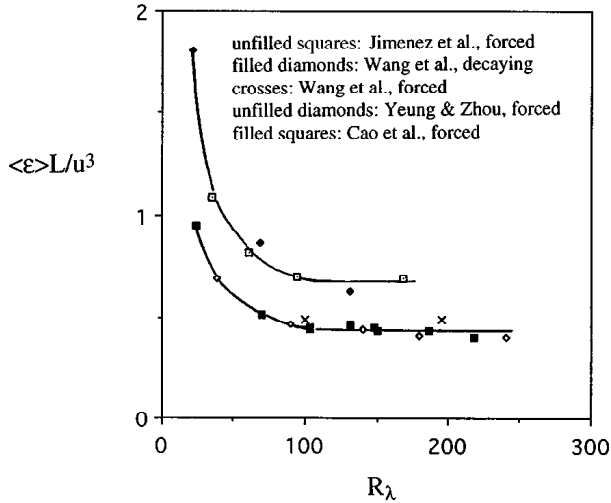


Figure 2.2: Variation of C_D as a function of Re number [24]

Moreover, Donzis et al. [25] analyzed DNS data on isotropic turbulence and found that the value of C_D in equation 2.39 tends to 0.4 as $Re_\lambda \rightarrow \infty$. These authors suggested the following equation for the rate of dissipation

$$\bar{\varepsilon} = A' \frac{u'^3}{L_{E,\parallel}} \left[1 + \sqrt{1 + \left(\frac{B'}{Re_\lambda} \right)^2} \right] \quad (2.42)$$

where $A' \approx 0.2$ and $B' \approx 92$.

DNS data analyzed by Yeung and Pope [26] indicate that the ratio of $(\bar{k}^{3/2}/\bar{\varepsilon}L_{E,\parallel})$ is increased from 2.29 to 4.12 when Re_λ is increased from 38 to 93. This would correspond to a reduction in the value of the C_D term of equation 2.39 from 0.85 to 0.45.

Additional DNS data analyzed by Yeung [27] suggest that the $(\bar{u}'^3/\bar{\varepsilon}L_L)$ ratio increases with Re_λ ; a value of around 3.2 was achieved at the largest simulated Reynolds number (which was about 220). This would correspond to a C_D value of approximately 0.3 if the Lagrangian length scale is substituted into equation 2.39.

This observed variation in the ratio of $u'^3/\bar{\varepsilon}L$ allows researchers to tune the dissipation rate in their simulations, which was also done in this work. Chapter 4 describes how varying the dissipation rate affected the results obtained, and explains how an optimal value was selected for validation.

The second source of uncertainty in RANS simulation relates to the turbulent Prandtl number, Pr_t . The turbulent Prandtl number is used to represent the ratio of the turbulent viscosity to heat diffusivity, $Pr_t = \nu_t/D_t$. In the framework of the k- ε model, D_t is defined by equation 2.25.

CHAPTER 2. TURBULENT COMBUSTION MODELING

The available data on the Pr_t number are controversial; typical values used in commercial CFD packages are 0.7 and 0.9, based on the work done by Spalding [28] and Launder [29], respectively.

However these values are not universally accepted. For example, Reynolds [30] argued that the Pr_t number depends on the ratio of the eddy and kinematic viscosities and the normal distance to the wall. Moreover, Koeltzsch [31] conducted wind tunnel experiments to examine a turbulent boundary layer above a flat plate and found out that the Sc_t number (i.e. the ratio of the turbulent viscosity to the mass diffusivity) ranged from 0.3 to 1.

Similarly, Flesch [32] reported that the mean value of the Sc_t number was 0.6 but that its standard deviation was 52%. In other words, their data indicated that the Sc_t number varies from 0.18 to 1.34. The authors suggested that some of this variation could be due to measurement uncertainty. However, they also argued that at least some of it was due to genuine variation in the Sc_t number.

Bilger et al. [33] obtained a value of $Pr = 0.35$ based on an experimental study of a reaction in a scalar mixing layer that was subject to grid-generated turbulence. Moreover, Yeung [27] has proposed equation 2.43

$$\widetilde{C}_0 = \frac{4}{3} \frac{\bar{k}\bar{\varepsilon}}{\tau_L} = \frac{8}{9} \frac{Pr_t}{C_\mu}, \quad (2.43)$$

\widetilde{C}_0 tends to take a value of 6.4 at large Reynolds numbers but is approximately halved at low Re numbers, which are common in laboratory experiments involving premixed turbulent flames. This would yield a relatively low value for the Pr_t number according to equation 2.43. For example, while $Pr_t = 0.65$ if $\widetilde{C}_0 = 6.4$, its value can be as low as 0.3 in non-reacting flows. It should be noted that the typical values for the Pr_t number, 0.7 and 0.9, were obtained by considering situations involving fully developed turbulent diffusivity that can be described by equation 2.25 under the assumption that $t \gg \tau_L$. However, since $t/\tau_L = O(1)$ for typical turbulent premixed flames, a lower Pr_t number should be used in the FSC model (in which the turbulent diffusivity is calculated according to equation 2.28) in order to achieve a diffusivity value equal to that predicted using equation 2.25 and a Pr_t value of 0.7.

Due to these uncertainties in the value of the Pr_t number, it is easy to justify tuning its value. Results obtained by such tuning are presented in chapter 4.

Chapter 3

Implementation of the models

3.1 Modification of the density calculation procedure in OpenFOAM

As discussed previously, within the framework of the BML approach, the density is calculated using equation 2.19. The turbulent premixed solver used in OpenFOAM is based on the combustion regress variable, $\tilde{b} = 1 - \tilde{c}$. One would therefore expect the density to be calculated according to equation

$$\frac{1}{\bar{\rho}} = \frac{1}{\rho_u} \tilde{b} + \frac{1}{\rho_b} (1 - \tilde{b}) \quad (3.1)$$

and the Favre-averaged temperature to be calculated as

$$\tilde{T} = T_u \tilde{b} + T_b (1 - \tilde{b}) \quad (3.2)$$

However, numerical simulations performed in the course of this work revealed that the Favre-averaged temperature yielded by the XiFoam solver with OpenFOAM(1.7.1)'s library differed significantly from that calculated using 2.19 or 3.1 in the middle part of a turbulent flame brush. These simulations focused on the geometrically simple test case shown in figure 3.1, with symmetry and outflow boundary conditions. Ignition is initiated in the corner of the system, which corresponds to the center of the domain if one accounts for the system's boundary conditions. The flame then propagates towards the outer boundaries. Methods for computing the density and temperature of the reacting mixture based on equations 3.1 and 3.2, respectively, were implemented explicitly in the solver. The results obtained using the newly-implemented method for calculating the density and that implemented in the original OpenFOAM were then compared. As shown in figure 3.2, the two methods yielded very different results.

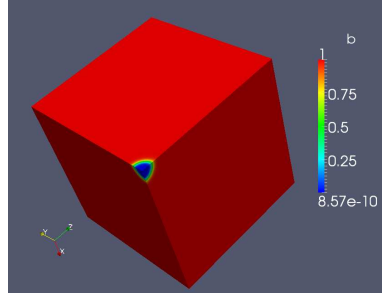


Figure 3.1: The simple geometric system used to evaluate the density and temperature calculated using the default and modified libraries, with ignition occurring at the center

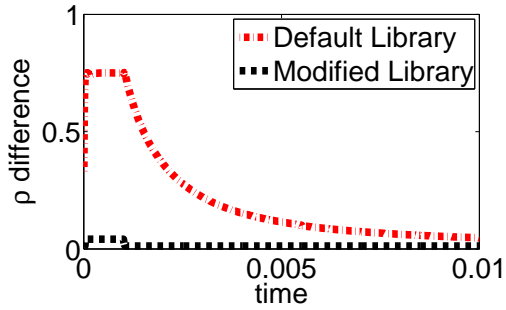


Figure 3.2: Variation in the normalized density over time (see equation 3.7) for the default and modified libraries

This section describes the origins of this problem and presents a method for solving it. In OpenFOAM, the temperature of the reacting mixture is calculated using the `janafThermoI.H` library based on the following equation

$$\begin{aligned}
 \frac{hM}{RT} &= \frac{H}{RT} = \sum_{k=1}^N \left(\frac{M}{M_k} Y_k \frac{H_k}{RT} \right) \\
 &= \sum_{k=1}^N \left[\frac{M}{M_k} Y_k \left(a_{1k} + \frac{a_{2k}}{2} T + \frac{a_{3k}}{3} T^2 + \frac{a_{4k}}{4} T^3 + \frac{a_{5k}}{5} T^4 + \frac{a_{6k}}{T} \right) \right] \\
 &= a_1 + \frac{a_2}{2} T + \frac{a_3}{3} T^2 + \frac{a_4}{4} T^3 + \frac{a_5}{5} T^4 + \frac{a_6}{T}
 \end{aligned} \tag{3.3}$$

where a_{jk} are the JANAF coefficients for the k -th specie, M is the molecular weight, Y_k is the mass fraction of the k -th specie, and the specific enthalpy $h = H/W$ of the mixture is evaluated by numerically integrating an appropriate balance equation. Equation 3.3 is well known to hold for multi-component mixtures. However, in OpenFOAM, it is applied to a

3.1. MODIFICATION OF THE DENSITY CALCULATION PROCEDURE IN OPENFOAM

fundamentally different situation in which the burned and unburned mixture are both present within the turbulent flame brush but are separated by a thin flamelet. More specifically, the mean state of the mixture within the flame brush is considered to be a “super-mixture” of the reactants and products. The mass fractions, Y_1 and Y_2 , respectively, of the reactants and products within this mixture are assumed to be \tilde{b} and, $1 - \tilde{b}$ respectively. Accordingly, the molecular weight M_m and JANAF coefficients a_{jm} for the super-mixture are initially determined as follows (see libraries homogeneous-Mixture.C, janafThermoI.H, specieI.H)

$$\frac{1}{M_m} = \frac{1}{M_r}\tilde{b} + \frac{1}{M_p}(1 - \tilde{b}) \quad \frac{a_{jm}}{M_m} = \frac{a_{jr}}{M_r}\tilde{b} + \frac{a_{jp}}{M_p}(1 - \tilde{b}) \quad (3.4)$$

The Favre-averaged temperature is then evaluated using the following equation (see libraries janafThermoI.H, specieThermoI.H)

$$\frac{\tilde{h}M_m}{R\tilde{T}} = a_{1m} + \frac{a_{2m}}{2}\tilde{T} + \frac{a_{3m}}{3}\tilde{T}^2 + \frac{a_{4m}}{4}\tilde{T}^3 + \frac{a_{5m}}{5}\tilde{T}^4 + \frac{a_{6m}}{\tilde{T}} \quad (3.5)$$

Table 3.1 compares the multi-component approach and the OpenFOAM approach. As was mentioned earlier, in the OpenFOAM approach, the mass fractions Y_1 and Y_2 for the reactants and products are replaced by the quantities \tilde{b} and $1 - \tilde{b}$, which originate from the description of multi-component mixtures.

Multi-component approach	OpenFOAM approach
$\frac{a_{m,k}}{M_m} = \sum_{l=1}^N a_{l,k} \frac{Y_l}{M_l}$	$\frac{a_{m,k}}{M_m} = \frac{a_{u,k}}{M_u}\tilde{b} + \frac{a_{b,k}}{M_b}(1 - \tilde{b})$
$\frac{1}{M_m} = \sum_{l=1}^N \frac{Y_l}{M_l}$	$\frac{1}{M_m} = \frac{1}{M_u}\tilde{b} + \frac{1}{M_b}(1 - \tilde{b})$
$h = \frac{R}{M_m} \left(\sum_{k=1}^5 \frac{a_{m,k}}{k} T^k + a_{m,6} \right)$	$\tilde{h} = \frac{R}{M_m} \left(\sum_{k=1}^5 \frac{a_{m,k}}{k} \tilde{T}^k + a_{m,6} \right)$

Table 3.1: Comparison of the multi-component and OpenFOAM approaches to calculating the temperature of the mixture

However, this approach has at least two important problems. First, multi-component gas mixtures are completely different to situations involving reactant-product intermittency within turbulent flame brushes, and

CHAPTER 3. IMPLEMENTATION OF THE MODELS

there is no justification for applying equation 3.3 in modeling the latter phenomenon. For example, all species within a multi-component gas have the same temperature, whereas $T_p \neq T_r$ in situations involving reactant-product intermittency is concerned. Moreover, the mean density of a multi-component mixture is calculated by

$$\rho = \sum_{k=1}^N \rho_k = \rho_u + \rho_b \quad (3.6)$$

However, as mentioned previously, in the BLM framework, the density of the mixture is calculated using equation 2.19; in the case where $T_p = T_r$, this method would predict a mean density of $\bar{\rho} = \rho_u = \rho_b$.

Second, the non-linear equation 3.3 does not commute with the process of taking a mean, i.e. the substitution of $\overline{\rho T^n}/\bar{\rho}$ with \bar{T}^n in the averaged equation 3.3 results in substantial errors.

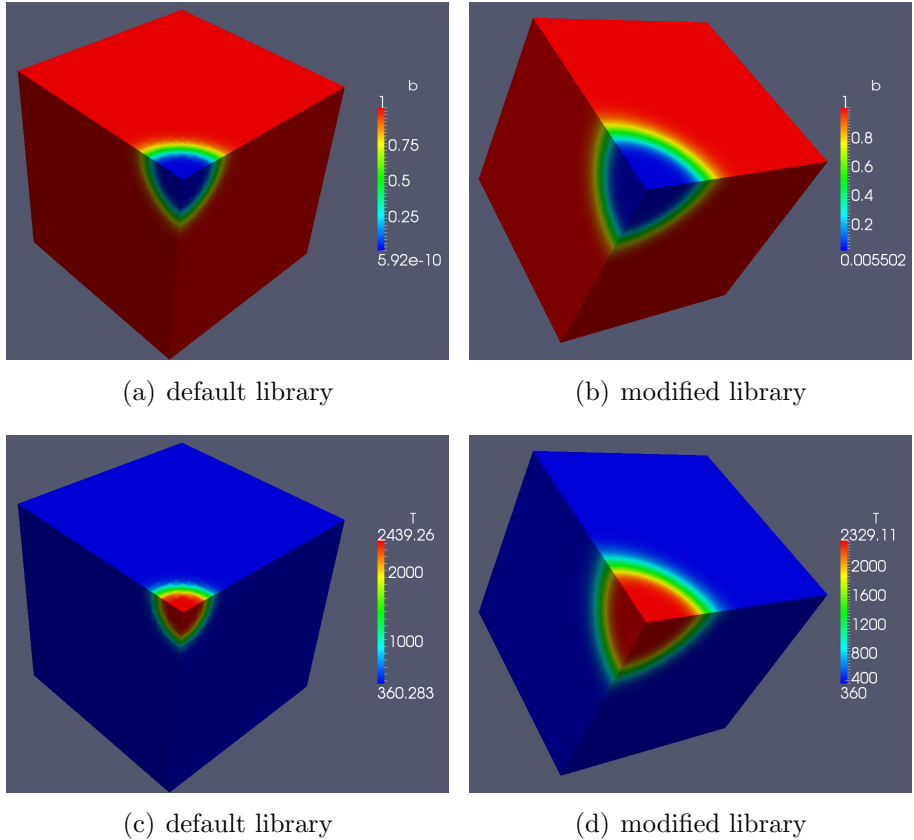


Figure 3.3: Comparison of the temperature and regress variable for the modified and default libraries

3.2. THE IMPLEMENTATION OF THE TFC AND FSC MODELS

To resolve this problem, the following method for evaluating \tilde{T} was implemented into the library hhuMixtureThermo.C of OpenFOAM. First, based on the local value of \tilde{h} obtained by numerically integrating an appropriate balance equation, the local values of T_u and T_b are determined by applying equation 3.3 to the pure reactants and pure products, respectively. That is to say, $T_u(T_b)$ is calculated using the reactant's (or product's) JANAF coefficients (see hhuMixtureThermo.C). Second, the Favre-averaged temperature is computed using equation 3.2.

The original and modified methods of calculating the Favre-averaged temperature and density, were compared by calculating the following relative error:

$$\delta\rho \equiv \max \left| \frac{\rho_{OF}(\mathbf{x}, t) - \bar{\rho}(\mathbf{x}, t)}{\bar{\rho}(\mathbf{x}, t)} \right| \quad (3.7)$$

Here, ρ_{OF} is the mean density obtained using the original OpenFOAM method; $\bar{\rho}$ is evaluated using equation 3.2, and the maximum is found in space at each time step. Typical results obtained in this way are shown in figure 3.2. It is readily apparent that the modified approach yields a much lower error than the original method, indicating that it is significantly more accurate.

Figure 3.3 shows the value of the temperature and the regress variable for both the default and the modified libraries. When using the default library, the position of the flame front identified by analyzing the distribution of temperatures is not the same as that determined by analysis of the regress variable. Conversely, the two flame fronts are identical when using the modified library.

The next chapter describes two sets of simulations that were performed assuming adiabatic conditions. Therefore, a simpler version of the code was implemented in which the enthalpy equation is not solved and the density is calculated directly according to equation 2.19, using ρ_u and ρ_b as input variables.

3.2 The implementation of the TFC and FSC models

The XiFoam solver in OpenFOAM(1.7.1) is based on the transport equation for the regress variable and solves enthalpy equations to calculate the unburned and burned temperatures. However, as mentioned in the previous section, the simulated test cases were based on the assumption of adiabatic conditions. Therefore, the unburned and burned temperature were treated

CHAPTER 3. IMPLEMENTATION OF THE MODELS

as input variables and there was no need to solve for the enthalpy. The default solver supplied with OpenFOAM was therefore modified in order to better describe adiabatic situations.

In addition, the TFC model (including equations 2.24 and 2.26) was implemented in OpenFOAM.

```
fvScalarMatrix bEqn
(
    fvm::ddt(rho, b)
    + mvConvection->fvmDiv(phi, b)
    + fvm::div(phiSt, b, "div(phiSt,b)")
    - fvm::Sp(fvc::div(phiSt), b)
//-----modified-----
    - fvm::laplacian(rho*Dt, b)
//-----End-----
);
```

where ρ is the modified density as discussed in the previous section, b is the regress variable, and ϕ is the velocity flux. $\rho * Dt$ is the turbulent diffusivity, which is calculated using equation 2.25 in the framework of the k- ε model, and ϕ_{St} is the turbulent flame speed flux; the turbulent flame speed is calculated using equation 2.29

```
Ut = A*up*pow(Da,0.25); // [m/s]
```

here, A is the model constant, up is the fluctuation in the velocity, and Da is the Damköler number.

In addition, the FSC model including equations 2.30, 2.29 and 2.28 was implemented in OpenFOAM as follows

```
fvScalarMatrix bEqn
(
    fvm::ddt(rho, b)
    + mvConvection->fvmDiv(phi, b)
    + fvm::div(phiSt, b, "div(phiSt,b)")
    - fvm::Sp(fvc::div(phiSt), b)
//-----modified-----
    - fvm::laplacian( rho*Dtt, b ) XX: laminar term
    + fvm::Sp(rho*Foam::exp(-activT/T_Tild)/(tr*(1+Dtt/alphab)), b)
//-----End-----
);
```

tr is the reaction time scale and ϕ_{St} is the turbulent flame speed flux. The turbulent flame speed and turbulent diffusivity are calculated using equations 2.29 and 2.28, respectively.

Chapter 4

Model validation

4.1 Introduction

Simulations of Spark Ignition(SI) engines are complicated since they use several complex physical models (such as turbulence and ignition models), and must deal with numerical problems such as those arising from the use of moving meshes and complicated geometries. This means that they allow for extensive tuning but also introduces multiple potential sources of error. Thus, while SI engine simulations are extremely useful for studying combustion processes, they are not by themselves sufficient for testing the performance of combustion models.

In order to further test the performance of the TFC and FSC models, they were therefore used to simulate two sets of experiments with simple geometry and wide range of fuel-air mixtures and substantially different operating conditions that have been reported in the literature. The simulated results were compared to those obtained in practice. The first set of experimental results was obtained during a study on oblique, confined, preheated (600 K) and highly turbulent CH₄-air flames with various equivalence ratios ($\Phi=0.62\text{-}1.24$) that was conducted by Moreau [1]. The second experimental data set was obtained from a series of measurements of open, weakly turbulent, lean ($\Phi=0.5$, 0.58, or 0.7) CH₄-air V-shaped flames formed under ambient conditions, and were performed by Dinkelacker and Hölzler [2].

4.2 Highly turbulent confined flames

4.2.1 Simulated test case

This section provides a brief description of the experimental studies that provided the data used to evaluate the performance of the models that were tested in this work. Figure 4.1 shows the experimental setup used by Moreau [1] to study turbulent confined flames generated in a high velocity flow of premixed methane and air. A gas-phase fuel was used in order to produce a more homogeneous mixture with air; methane was selected because it could be injected at high pressure. The methane-air mixture was preheated to 600 K because it was difficult to achieve stable combustion at lower temperatures when using high flow velocities. The mixture was ignited and stabilized using an auxiliary hot pilot flow that ran parallel to the main cold stream. Three different configurations were used in the experiment in order to vary the level of turbulent intensity at the inlet. Main flow equivalence ratios ranging from 0.62 to 1.24 were investigated, and information on the location of the flame front was gathered using both direct and shadowgraph methods. The thickness of the reaction zone was determined by conducting local temperature measurements and by gas sampling [1].

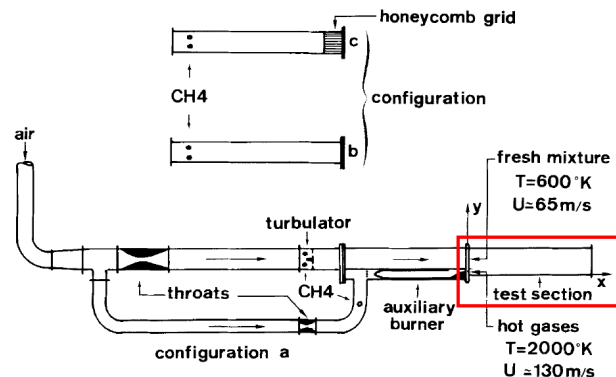


Figure 4.1: The experimental setup used by Moreau [1]

Combustion chamber with 1300 mm long and with a 100 × 100 mm cross section was simulated in two dimensional. The location of the combustion chamber is indicated by the red box in figure 4.1 and is also shown in figure 4.2. The main and pilot flows were separated by a thin splitter to prevent recirculation. The heights of the pilot and main flows were 20 mm and 80 mm, respectively, with mean flow velocities of 60 and 120 m/s, respectively. These conditions generated intense turbulence with a high Da value; such conditions are typical in industrial burners. Because of this factor together

4.2. HIGHLY TURBULENT CONFINED FLAMES

with the simple geometry of the experimental system and the wide range of equivalence ratios that were tested in experiments, many researchers have used Moreau's experimental results as a source of reference data to support computational and numerical studies.

Various groups have conducted numerical analyses of the Moreau experiments. For instance, Borghi and Moreau [34] simulated this test case (but only considered a single equivalence ratio, $\Phi = 0.84$) using a probability function to describe changes in the temperature of the system and assuming a single step global reaction. Maciocco and Zimont [35] performed simulations using the TFC model for equivalence ratios of 0.8 and 0.84 with a Pr_t value of 0.7. Zimont and Battaglia [36] examined one of the experimentally tested equivalence ratios using RANS/LES in conjunction with the TFC model. Finally, Ghirelli [37] simulated the experiment at an equivalence ratio of 0.8 using the TFC model with $Pr_t = 0.7$ and compared the results obtained to those achieved with a model he has developed that is based on the new dispersion model [38].

In this work, the Moreau experiments were simulated using the TFC and FSC models. Simulations were performed for all of the experimentally studied equivalence ratios (i.e. $\Phi=0.62 - 1.24$) in order to validate the models under a wide range of conditions. The turbulent Prandtl number and dissipation rate were tuned to match the experimental data at an equivalence ratio of $\Phi = 0.8$ and the resulting tuned values were used in all subsequent simulations regardless of the equivalence ratio. More details concerning the numerical aspects of the simulations are presented below.

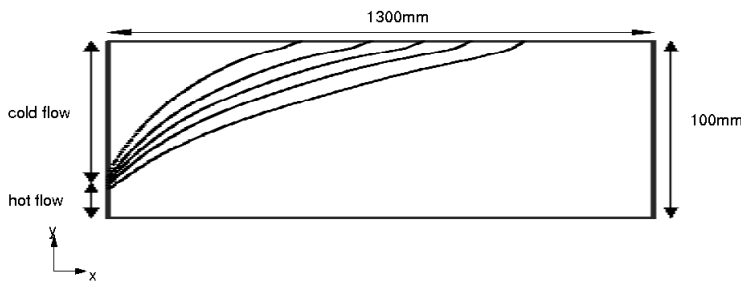


Figure 4.2: Schematic of the Moreau simulated test case

4.2.2 Numerical setup

Two-dimensional simulations of the Moreau experiments were set up using both the TFC and FSC models, which are outlined in chapter 2 with the standard $k - \epsilon$ model [39]. Dependency of the results to the mesh size was investigated by performing preliminary runs with different meshes ($650 \times$

CHAPTER 4. MODEL VALIDATION

50, 1300×120); ultimately, a uniform 325×25 grid was identified as being optimal and was used in all of the simulations discussed below.

A range of numerical discretization schemes for the divergence term were investigated but it was found that the results obtained were independent of the scheme used, so the limited second order central difference method was selected for the convection term discretization.

	$T(K)$	$k(m^2/s^2)$	c	$U(m/s)$	$\rho(kg/m^3)$
cold flow	600	100	0	60	0.5603
hot flow	$T(\Phi)$	793	1	120	$\rho(\Phi)$

Table 4.1: Inflow boundary conditions

The inflow boundary conditions are specified in table 4.1. Values for the kinetic energy were taken from the work of Maciocco and Zimont [35]. These values were determined at a position located 39 mm away from the inlet. Wall functions and outflow boundary conditions were set at the other boundaries. The values for dissipation rate and turbulent Prandtl number were tuned; the tuning process is discussed in section 2.8.

Simulations were performed for all of the equivalence ratios for which experimental data were available, i.e. at ratios ranging from 0.62 to 1.24. The corresponding laminar flame speeds (see table 4.2) were calculated using the Premixed code [40] with the GRI 3 mechanism [41]. The burned temperature, T_b , unburned and burned viscosity ν_u, ν_b unburned and burned thermal diffusivity, κ_u, κ_b were computed using the Chemkin code [42]; the calculated values for these parameters are shown in table 4.2.

Φ	0.62	0.80	0.83	0.85	0.87	1	1.24
$T_b[K]$	1935	2200	2235	2258	2279	2373	2311
$\rho_u[kg/m^3]$	0.5645	0.5603	0.5596	0.5591	0.5587	0.5557	0.5505
$\rho_b[kg/m^3]$	0.175	0.1524	0.1496	0.1479	0.1463	0.1386	0.1365
$\nu_u[m^2/s]$	5.25e-5	5.26e-5	5.26e-5	5.27e-5	5.27e-5	5.27e-5	5.29e-5
$\nu_b[m^2/s]$	3.72e-4	4.63e-4	4.76e-4	4.85e-4	4.93e-4	5.33e-4	5.32e-4
$\alpha_u[m^2/s]$	7.38e-5	7.39e-5	7.39e-5	7.39e-5	7.39e-5	7.40e-5	7.41e-5
$\alpha_b[m^2/s]$	5.25e-4	6.57e-4	6.76e-4	6.88e-4	7.01e-4	8.01e-4	8.00e-4
$S_L[m/s]$	0.7	1.13	1.18	1.21	1.24	1.35	1.17
$t_0[ms]$	1.33e-5	6.40e-6	6.06e-6	5.56e-6	5.06e-6	5.24e-6	6.82e-6

Table 4.2: Input data for the simulations of the Moreau experiments

4.2.3 Results, validation, and discussion

The discussion of the results obtained in this work is subdivided into three main sections, covering:

- i) sensitivity analysis,
- ii) tuning
- iii) validation.

The first section describes investigations into the sensitivity of the results to three-dimensional effects, the identity of the turbulence model used, and the velocity used to calculate the flame development time in the FSC model, $t = x/u$. As discussed extensively in section 2.8, it was necessary to tune the values of Pr_t and ε that were used in the simulations. The second section explains the procedure used to tune these parameters for the TFC and FSC models, which involved considering a single equivalence ratio and varying their values to identify those that yielded the closest agreement with the experimental data in each case. The final section describes the results obtained in the simulations conducted for other equivalence ratios using the tuned values for Pr_t and the dissipation rate. The specific topics discussed in each section are listed below:

- Sensitivity Analysis:
 1. A comparison of 2D and 3D simulations using the TFC model
 2. The effect of varying the turbulence model on TFC simulations
 3. The effect of varying the velocity parameter used to compute $t = x/u$ in the FSC model
- Tuning:
 4. Effect of varying the dissipation rate on TFC simulations
 5. Effect of varying the dissipation rate on FSC simulations
 6. Effect of varying the Pr_t number on TFC simulations
 7. Effect of varying the Pr_t number on FSC simulations
- Validation:
 8. Comparison of the simulated results obtained using the TFC and FSC models, and the FSC model with an exponential source term

CHAPTER 4. MODEL VALIDATION

- Sensitivity Analysis:

1. A comparison of 2D and 3D simulations using the TFC model

Preliminary three-dimensional simulations were performed to determine whether there were any important differences between their results and those obtained in 2D simulations. As can be seen in figure 4.3, the results in the two cases were very similar; therefore, to reduce computational costs, all of the subsequent simulations were two-dimensional.

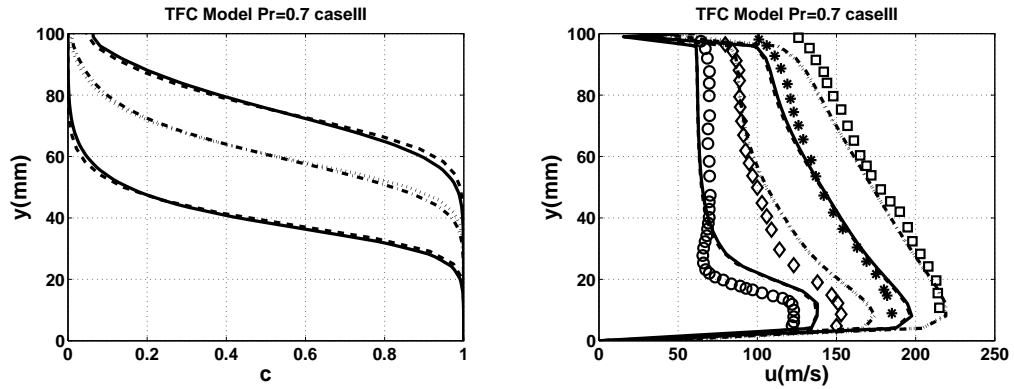


Figure 4.3: Comparison of the predicted \tilde{c} and velocity profiles obtained in 2D and 3D simulations using the TFC model at $\phi = 0.80$ (simulated results are shown as continuous lines, experimental data points are indicated by symbols)

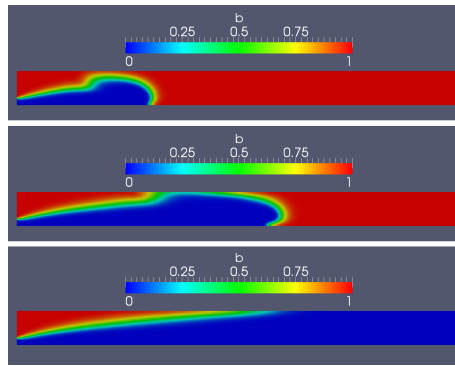


Figure 4.4: Development of the flame within the combustion chamber

The flame development along the combustion chamber in 2D case is shown in figure 4.4 by visualizing the regressing variable field which is defined as $\tilde{b} = 1 - \tilde{c}$.

4.2. HIGHLY TURBULENT CONFINED FLAMES

- Sensitivity Analysis:

2. The effect of varying the turbulence model on TFC simulations

In order to investigate the sensitivity of the results to the turbulence model, simulations were performed using four different turbulence models - specifically, the $k - \varepsilon$ [39], *Launder Sharma* [43], *RNG* [44] and *realizable k - e* [45] models. Figures 4.5 and 4.6 show the transversal profiles of the progress variable and the magnitude of the velocity at different positions within the combustion chamber using the different turbulence models.

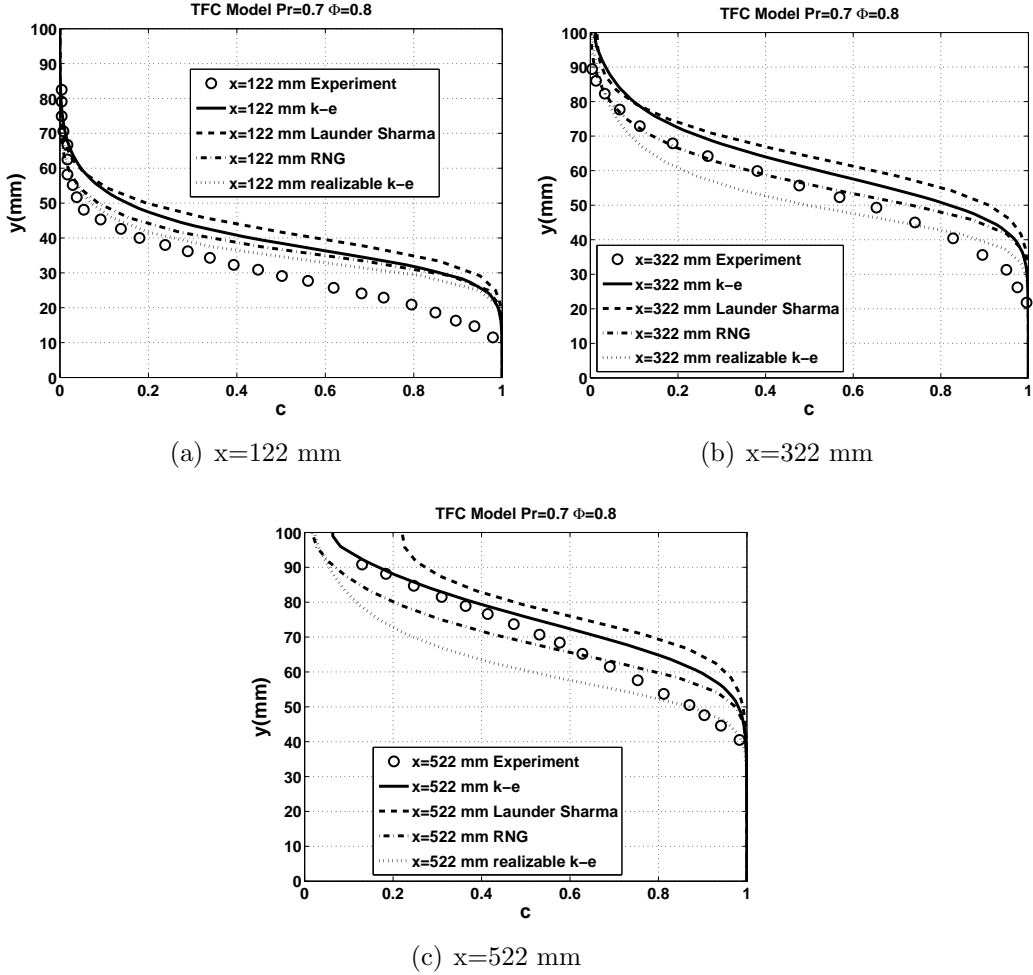


Figure 4.5: \tilde{c} transversal profiles obtained using different turbulence models in TFC simulations at $\phi = 0.8$ and $Pr = 0.7$

Simulations conducted using the TFC model at $\Phi = 0.8$ and $Pr_t = 0.7$ with a case III-type dissipation rate (for an explanation of this terminology,

CHAPTER 4. MODEL VALIDATION

see table 4.3). The \tilde{c} profile clearly shows that the burning rate and flame brush thickness are both sensitive to the turbulence model used.

Figure 4.5 shows that the Launder Sharma model consistently predicts higher burning rates than are obtained with the other turbulence models. Moreover, the predicted burning rates generated using this model tend to be significantly greater than the experimental values. The realizable $k - \epsilon$ model tends to predict relatively low burning rates, while the rates predicted by the $k - \epsilon$ and RNG models are intermediate between these two extremes. It is also apparent that the realizable $k - \epsilon$ model underpredicts the burning rate at the 322 mm and 522 mm positions. Overall, the results obtained using the RNG and $k - \epsilon$ models are closest to the experimental results.

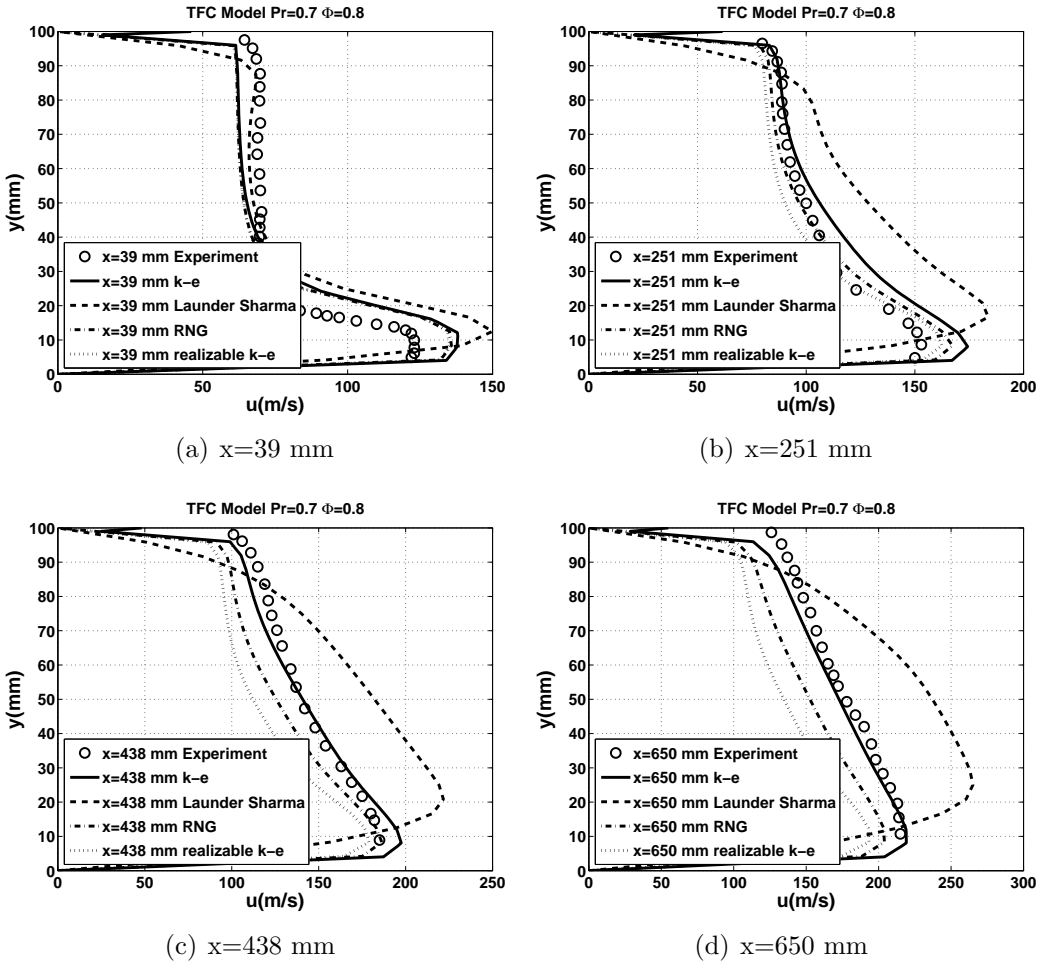


Figure 4.6: Transversal profiles of the velocity magnitude obtained using different turbulence models in TFC simulations at $\phi = 0.8$ and $Pr = 0.7$

It should be mentioned that the values of the Pr_t number and dissipation

4.2. HIGHLY TURBULENT CONFINED FLAMES

rate had not been tuned at this point in the study, and it is possible that the use of tuned parameters might significantly affect the performance of the tested models.

The streamwise velocity profiles shown in figure 4.6 show that the Lauder Sharma model overpredicts the magnitude of the flow velocity at the 251 mm, 438 mm and 650 mm positions. Moreover, both the realizable $k-\epsilon$ model and the RNG model underpredict the magnitude of the velocity at the 438 mm and 650 mm positions. Overall, the results obtained with the $k-\epsilon$ model seem to have the best agreement with the experimental data.

The $k-\epsilon$ model performed better than the alternatives in terms of predicting both the burning rate and the magnitude of the velocity and was therefore used in all subsequent simulations.

- Sensitivity Analysis:

3. The effect of varying the velocity parameter used to compute $t = x/u$ in the FSC model

As discussed in chapter 2 and as shown by equations 2.29 and 2.28, the turbulent flame velocity and turbulent diffusivity are functions of time in the FSC model. However, the work presented herein focused on time-independent stationary cases. It was therefore necessary to redefine t in the FSC model. As was discussed in section 2.8, this was done by assuming that $t = x/u$ where x is the distance from the flame holder (or splitter in this case) and u is the mean velocity.

The sensitivity of the FSC model to the value of the velocity parameter was investigated by using both the burned and the unburned velocity to calculate t (using $t = x/u$) in simulations performed with this model. The values for the burned and unburned velocities in this case are 120 m/s and 60 m/s, respectively, as shown in table 4.1. In both cases, the simulated equivalence ratio was 0.8 and the value of Pr_t was 0.3. As can be seen in figure 4.7, the results for $x=122$ mm were relatively insensitive to the velocity. However, the divergence in the results became more pronounced further downstream (i.e. at greater distances from the splitter), as can be seen in figure 4.7 *b* and *c*. That is to say, the results became more sensitive to the inlet velocity, specially on the unburned side ($\tilde{c} \simeq 0$). A velocity of 120 m/s was assumed in all of the subsequent FSC simulations.

CHAPTER 4. MODEL VALIDATION

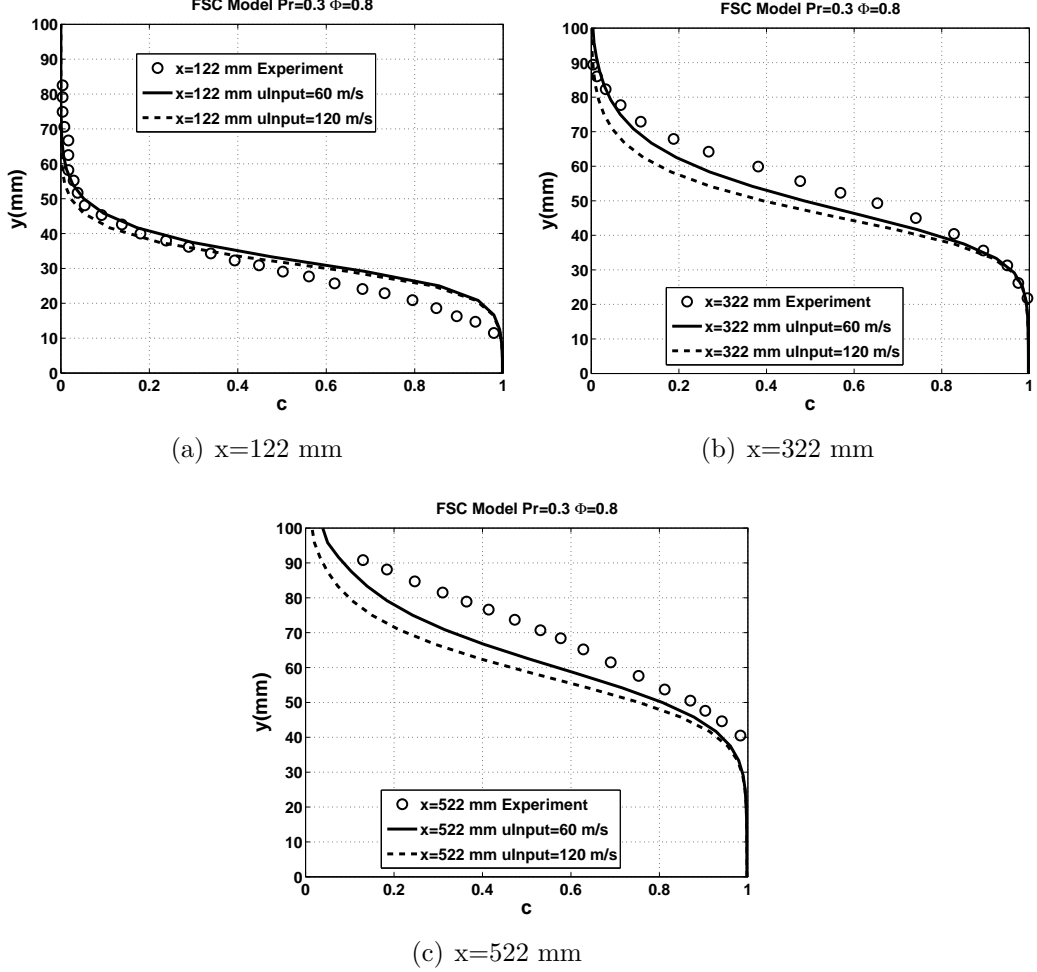


Figure 4.7: Sensitivity of the FSC model to the velocity used to calculate $t = x/u$ at $\phi = 0.8$ and $\text{Pr} = 0.3$

- Tuning:

4. Effect of varying the dissipation rate on TFC simulations

As mentioned in section 2.8, the length scale is generally not defined exactly in the experimental literature on turbulent combustion. In addition, the constant C_D in equation 2.39 depends on the Reynolds number. It is therefore necessary to manually tune the value of the dissipation rate when performing simulations in order to achieve good agreement with the available experimental data.

Moreau [1] did not report length scale data for his experiments, and a range of values for this parameter have been assumed in previous computational studies that used his work as a source of reference data. Therefore,

4.2. HIGHLY TURBULENT CONFINED FLAMES

simulations of the Moreau experiments at an equivalence ratio of 0.8 were performed using each of the four different length scales listed in table 4.3 in order to identify an appropriate value for this parameter in subsequent TFC simulations. The four length scales are labeled cases I-IV to facilitate discussion.

	case I	case II	case III	case IV
$l_u[\text{mm}]$	24	8.21	5.4	2.7
$l_b[\text{mm}]$	6	1.83	1.6	0.8
$\varepsilon_u \text{m}^2/\text{s}^3$	6.85e3	2e4	3.7e4	7.4e4
$\varepsilon_b \text{m}^2/\text{s}^3$	6.12e5	2e6	2.86e6	5.6e6

Table 4.3: The four different length scales considered and the associated inflow dissipation rates in (m^2/s^3)

The dissipation rates associated with each of the four tested length scales shown in table 4.3 were calculated using equation 2.39. The length scale used in case I is that reported by Zimont et.al [13]. Cases II and III assume length scales based on the work of Ghirelli [37] and Maciocoo and Zimont [35], respectively. It should be noted here that Ghirielli considered non-isotropic turbulence in the study from which the case II length scale was taken and therefore obtained a different value for the kinetic energy than was found in this work. The length scale used in case IV was chosen arbitrarily and is twice that used in case III.

In order to investigate the effect of the dissipation rate on the TFC model, TFC simulations were conducted assuming Pr_t values of 0.3 and 0.7 at an equivalence ratio of $\Phi = 0.80$ using dissipation rates presented in table 4.3. Figure 4.8 shows the results obtained at different positions within the combustion chamber (i.e. at different values of x) in each case. As the dissipation rate was increased on going from case I to case IV, the level of turbulent diffusion (which was calculated using equation 2.25) decreased. This caused a decrease in the mean flame brush thickness, with a corresponding increase in the slopes of the curves shown in figure 4.8. As described by equation 2.39, increases in the the dissipation rate are associated with decreases in the length scale of the system, which in turn reduce the Da number ($\frac{\tau_t}{\tau_c} = \frac{L/u'}{\tau_c}$). This reduces the burning rate, as described by equation 2.26. Results consistent with these expectations were obtained at all positions within the combustion chamber, at both tested values of the Prandtl number. A summary of these trends is given by equations 4.1 and 4.2.

$\varepsilon \uparrow \implies D_T \downarrow \implies \text{Thickness} \downarrow$

(4.1)

CHAPTER 4. MODEL VALIDATION

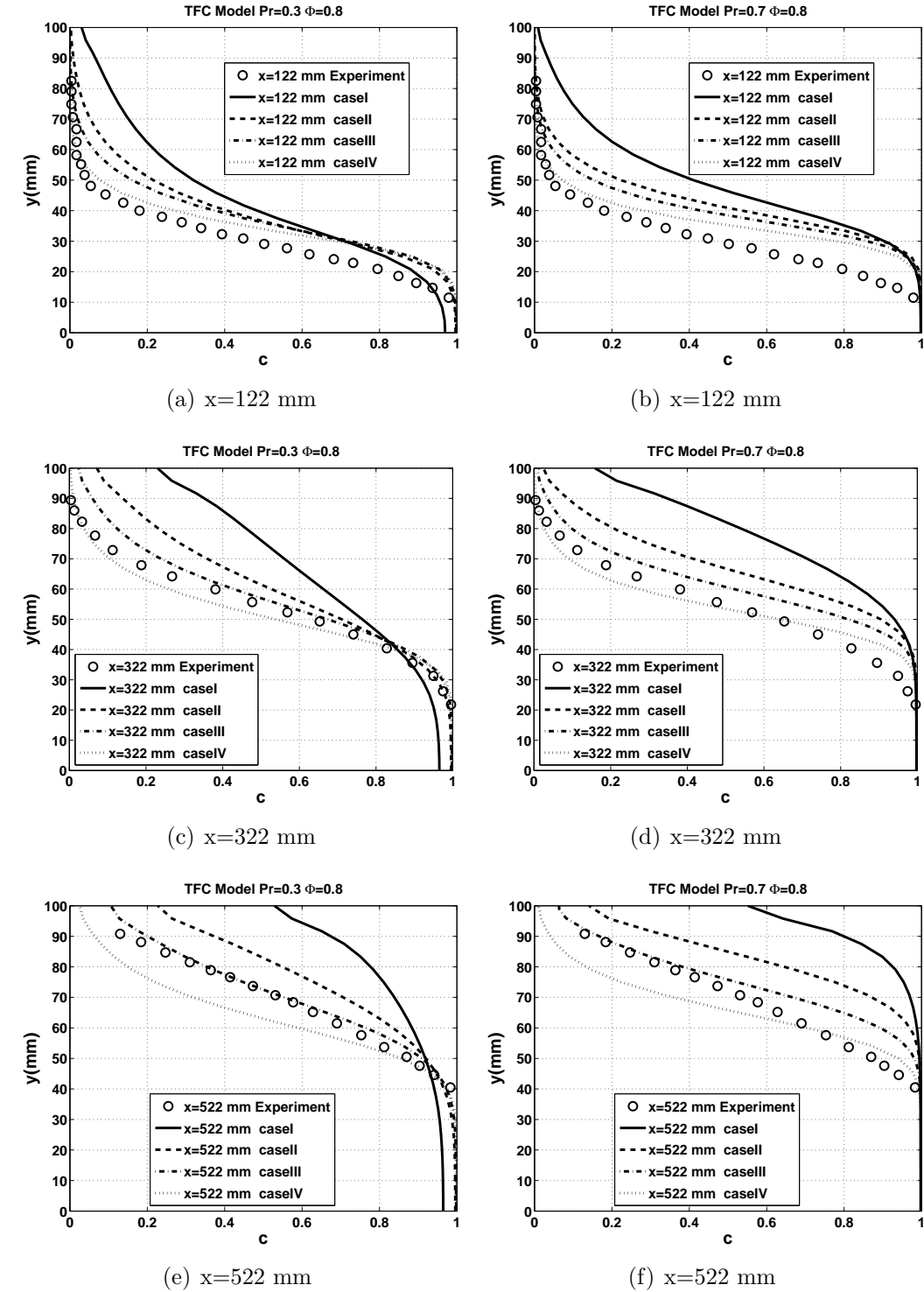


Figure 4.8: The effect of varying the dissipation rate on the \tilde{c} transversal profile obtained using the TFC model at $\phi = 0.8$ for Pr_t values of 0.3 and 0.7

$$\boxed{\varepsilon \uparrow \implies L \downarrow \implies Da \downarrow \implies \text{Burning rate} \downarrow} \quad (4.2)$$

The simulated \tilde{c} values were greater than the experimental values at the $x = 122$ mm position for all tested dissipation rates and Pr_t values. Overall, however, the case III length scale yielded the simulated results that agreed most closely with the experimental data. The case III length scale was therefore used in TFC in all the other equivalence ratio simulations. Therefore case III length scale was selected for TFC model to simulate all other subsequent equivalence ratios.

- Tuning:

5. Effect of varying the dissipation rate on FSC simulations

With the similar discussion as made in section 2.8, dissipation rate required tuning. Therefore the same dissipation rates presented in table 4.3 were used to investigate the effects of dissipation rate on turbulent burning rate and also flame brush thickness using FSC model with $Pr_t = 0.3$ on a single equivalence ratio equal to 0.8. Moreover another purpose of this analysis is to find the dissipation rate which gives the best agreement with experimental data, and use that value to simulate other equivalence ratios. The effects of dissipation rate on transversal profile of \tilde{c} is presented in figure 4.9 for a different sections along x direction.

The effects of varying the dissipation rate on the \tilde{c} profiles obtained in the FSC simulations were similar to but less pronounced than those observed for the TFC model. The progressive increase in the dissipation rate on going from case I to case IV caused a decrease in the turbulent diffusivity as predicted by equation 2.28, which in turn reduced the flame brush thickness. This effect is indicated by the gradual increase in the slope of the curves for cases I to IV in figure 4.9. The observation that the effect is less pronounced than was the case for the TFC simulations can be explained by considering the time-dependent term in the turbulent diffusivity equation used in the FSC model (equation 2.28).

Increasing the dissipation rate will decrease the fully developed turbulent diffusivity, which is calculated using equation 2.25. However, it also decreases the value of the $\tau_L = D_{t,\infty}/u'^2$ term of equation 2.28 and thereby increases the value of the time-dependent term, $[1 - \exp(-\frac{t_{fd}}{\tau_L})]$. This trend is shown analytically in figure 4.10(a)

Overall, since $D_{t,\infty}$ decreases and the time-dependent term $[1 - \exp(-\frac{t_{fd}}{\tau_L})]$ increases, the total turbulent diffusivity will decrease but to a lesser extent

CHAPTER 4. MODEL VALIDATION

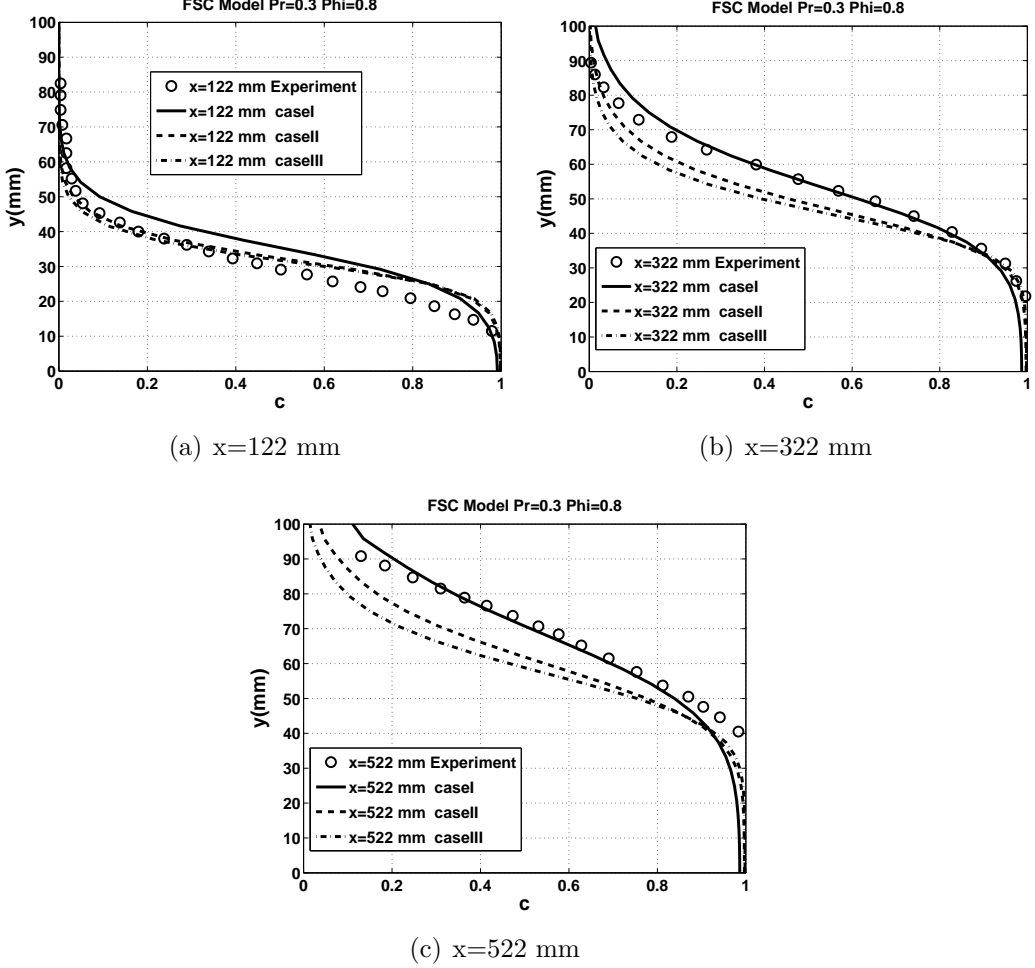


Figure 4.9: The effect of varying the dissipation rate on the \tilde{c} transversal profile obtained using the FSC model at $\phi = 0.8$ for a Pr_t value of 0.3

than would occur in the TFC model and therefore decrease the turbulent flame brush thickness. This trend is summarized by equation 4.3.

$$\varepsilon \uparrow \implies D_{T,\infty} \downarrow \implies \tau_L \downarrow \implies \text{Thickness} \downarrow \text{ (less pronounced)} \quad (4.3)$$

As was the case for the turbulent diffusivity, the relationship between the assumed dissipation rate and the burning rate in the FSC simulations was similar to but less pronounced than that seen in the TFC simulations. The length scale decreases as the dissipation rate increases. This causes a decrease in $\tau_t = L/u'$, which in turn reduces $Da = \tau_t/\tau_c$. The decrease in the Da number reduces the value of $U_{t,\infty}$ as described by equation 2.26.

4.2. HIGHLY TURBULENT CONFINED FLAMES

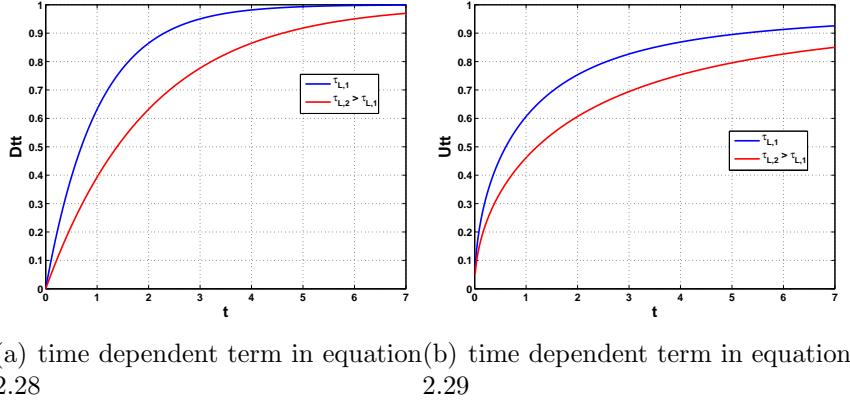


Figure 4.10: Variation of time dependent terms in FSC model by varying a τ_L

However, in the FSC model, the time-dependent exponential term plays an important role. Increases in the dissipation rate cause the $\tau_L = D_t/u^2$ component of this term to decrease because of the associated decrease in $D_{t,\infty}$. This effect is analytically shown in figure 4.10(b). That is to say, the magnitude of the time-dependent term increases with the dissipation rate. Overall, then, increasing the dissipation rate decreases the value of $U_{t,\infty}$ but increases the time-dependent term. The net result is a reduction in $U_{t,t}$ as described by equation 4.4. However, this effect is less pronounced than in TFC simulations. This trend is summarized by equation 4.4.

$$\boxed{\varepsilon \uparrow \implies L \downarrow \implies U_{t,\infty} \downarrow \implies \tau_L \downarrow \implies \text{Burning rate} \downarrow \text{(less pronounced)}} \quad (4.4)$$

Figure 4.9 clearly shows that the case I dissipation rate gives the best agreement with the experimental results in simulations using the FSC model. This dissipation rate was therefore assumed in all subsequent FSC simulations for all other equivalence ratios.

- Tuning:

6. The effect of varying the Pr_t number on TFC simulations

As discussed in section 2.8, there is some controversy regarding the value of the turbulent Prandtl number Pr_t . While Pr_t is commonly assumed to be 0.7 or 0.9, significantly lower Pr_t were used in many simulations reviewed elsewhere [27], [33]. Investigations were therefore conducted to determine how varying the Pr_t affected the results obtained in TFC simulations and to identify the Pr_t number that would yield the closest agreement with

CHAPTER 4. MODEL VALIDATION

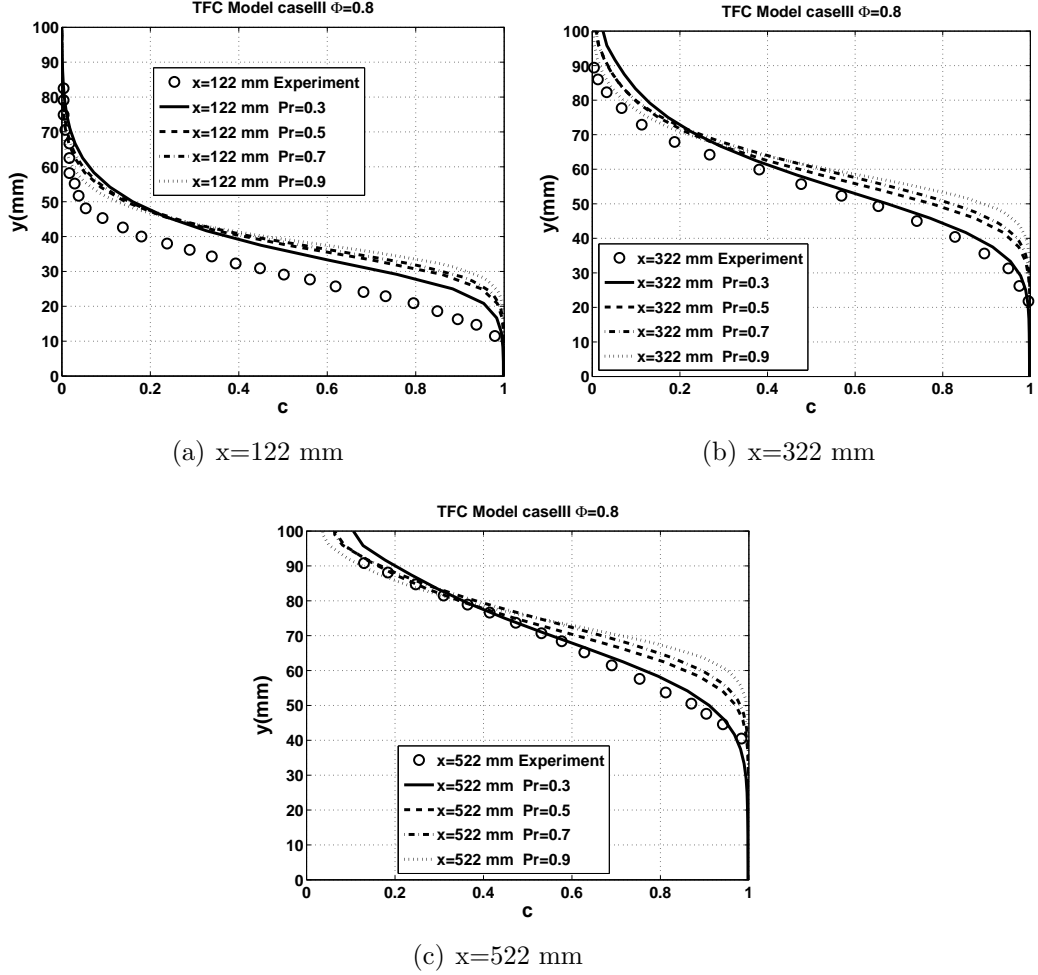


Figure 4.11: The effect of varying the Pr_t number on the \tilde{c} profile obtained in TFC simulations at $\phi = 0.80$ using the case III dissipation rate

the experimental data. This was done by performing TFC simulations of the Moreau experiments at an equivalence ratio of $\Phi = 0.8$ using the case III dissipation rate (see Table 4.3) and four different Pr_t numbers. Figure 4.11 shows how \tilde{c} varied along y direction for different sections within the combustion chamber. Increasing the Pr_t number increases the slope of the \tilde{c} curve, which corresponds to a decrease in the turbulent flame brush thickness. This occurs because of the associated decrease in the turbulent diffusivity, as predicted by equation 2.25.

The data presented in figure 4.11 indicate that the results obtained using a Pr_t value of 0.3 were more consistent with the experimental data than were those obtained with the more commonly used value of 0.7. However,

4.2. HIGHLY TURBULENT CONFINED FLAMES

since it has been reported that the latter value is more appropriate for use in TFC simulations, both values were used in subsequent investigations using the TFC model.

- Tuning:

7. The effect of varying the Pr_t number on FSC simulations

As discussed in the preceding section and in section 2.8, there has been some controversy regarding the value of the Pr_t number and different groups used different values. It was therefore necessary to determine how the Pr_t value affects the results obtained in FSC simulations and to identify the value that yields the best agreement with the available experimental data.

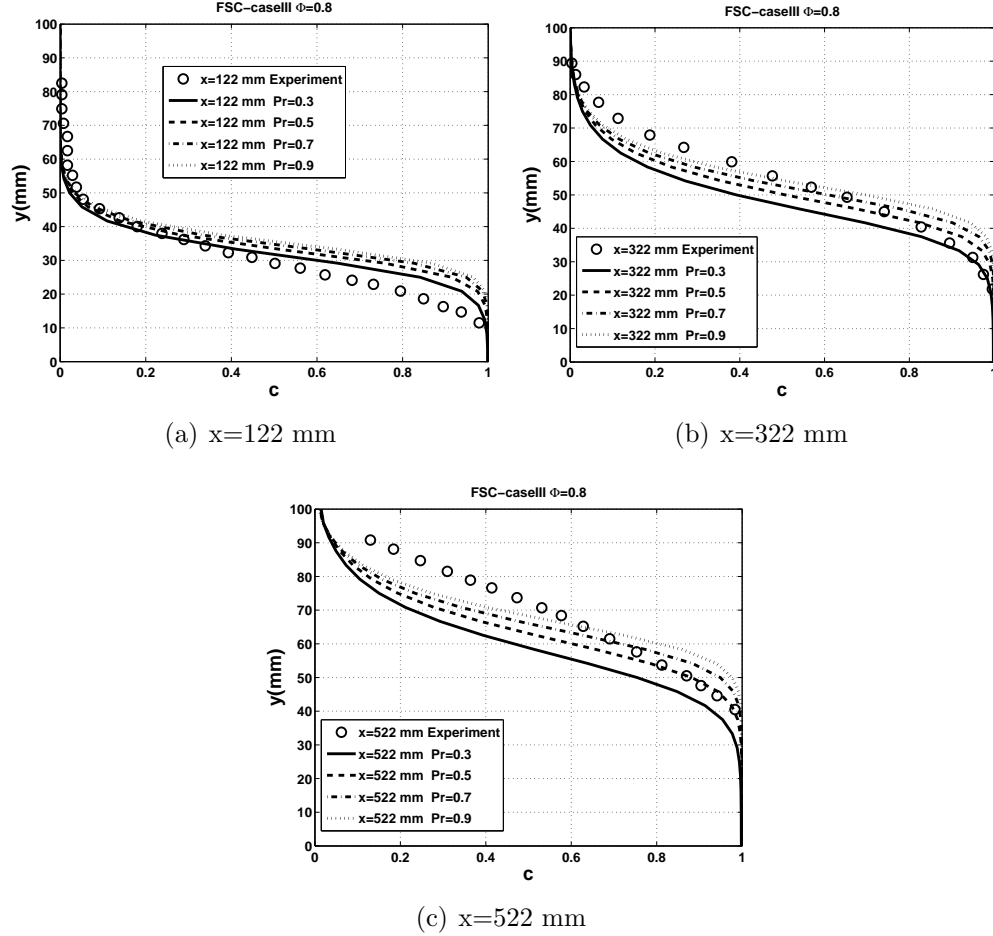


Figure 4.12: The effect of varying the Pr_t number on the \tilde{c} profile obtained in FSC simulations at $\phi = 0.80$ using the case III dissipation rate

CHAPTER 4. MODEL VALIDATION

FSC simulations of the Moreau experiment at an equivalence ratio of 0.8 were therefore conducted using four different Pr_t values and the case III dissipation rate (see table 4.3). Figure 4.12 shows transversal profile of \tilde{c} along y direction for different sections along combustion chamber.

Increasing the Pr_t number decreases the turbulent diffusivity according to equation 2.28 and therefore decreases the flame brush thickness, which in turn increases the slope of the \tilde{c} profile. Increases in the Pr_t number also reduce the turbulent Lagrangian time scale, $\tau_L = \frac{D_{T,\infty}}{u'^2}$. This increases the t_{fa}/τ_L ratio, which in turn increases the turbulent burning rate. (equation 2.29)

It is readily apparent that the simulations using a Pr_t value of 0.3 gave the closest agreement with the experimental data. Moreover, in keeping with the findings presented previously, the simulated burning rate were in closer agreement with the experimental results when the case I dissipation rate was used. A Pr_t value of 0.3 was therefore used in all subsequent simulations conducted using the FSC model.

- Validation:

- 8. Comparison of the simulated results obtained using the TFC and FSC models, and the FSC model with an exponential source term

The tested models (TFC, FSC, and FSC with an exponential source term) were validated by simulating the Moreau experiments at wide range of equivalence ratios using the tuned values for the dissipation rate and Pr_t number that were identified by considering the $\Phi = 0.8$ case. That is to say, the TFC simulations were conducted assuming the case III dissipation rate and a Pr_t value of 0.3, while the FSC simulations were conducted assuming the case I dissipation rate and a Pr_t value of 0.3. The same values of Prandtl number and dissipation rate used in the FSC simulations were also used in the simulations performed using the FSC model with an exponential source term. In addition, simulations were performed using the TFC model with the conventional Pr_t value of 0.7.

Subfigures 4.13 a, c, and e show the simulated \tilde{c} transversal profiles obtained for the leanest case studied by Moreau ($\Phi = 0.62$). It is clear that when using the TFC model, the tuned Pr_t value of 0.3 gives results that agree more closely with the experimental data than are obtained using the conventional value of 0.7. Moreover, TFC simulations with a Pr_t value of 0.7 yield the lowest predicted flame brush thicknesses because the high Pr_t number and dissipation rate reduce the predicted turbulent flame diffusivity.

The simulations using the FSC and FSC with exponential source term models also produced results that were in good agreement with the experimental data for the $\Phi = 0.62$ case. However, the FSC model did not

4.2. HIGHLY TURBULENT CONFINED FLAMES

accurately reproduce the experimental $\tilde{c} = 1$ value at positions further downstream (i.e. at large values of x) due to numerical errors. This problem was solved by adding an extra source term to the \tilde{c} equation, i.e. by introducing an exponential source term into the FSC model.

The simulated results for the $\Phi = 0.8$ case are shown in subfigures 4.13 b, d, and f. The simulated data for all of the tested models are in good agreement with the experimental results at all positions within the combustion chamber. However, the results obtained using the TFC with the tuned Pr_t value of 0.3 are in better agreement with the experimental data than are those obtained using the conventional value of 0.7. In addition, the predicted flame brush thickness obtained using the TFC model under the assumption that $Pr_t = 0.7$ was relatively low.

Figures 4.14 and 4.15 show the simulated \tilde{c} transversal profiles for equivalence ratios of 0.83, 0.85, 0.87, 1 and 1.24. These results were obtained without any additional tuning and are in good agreement with the experimental data. It is apparent that all of the models slightly overestimate the value of \tilde{c} in the $x=122$ mm section. Moreover, in the richest case, the value of \tilde{c} is consistently overestimated by all models, although the agreement with the experimental data remains acceptable.

CHAPTER 4. MODEL VALIDATION

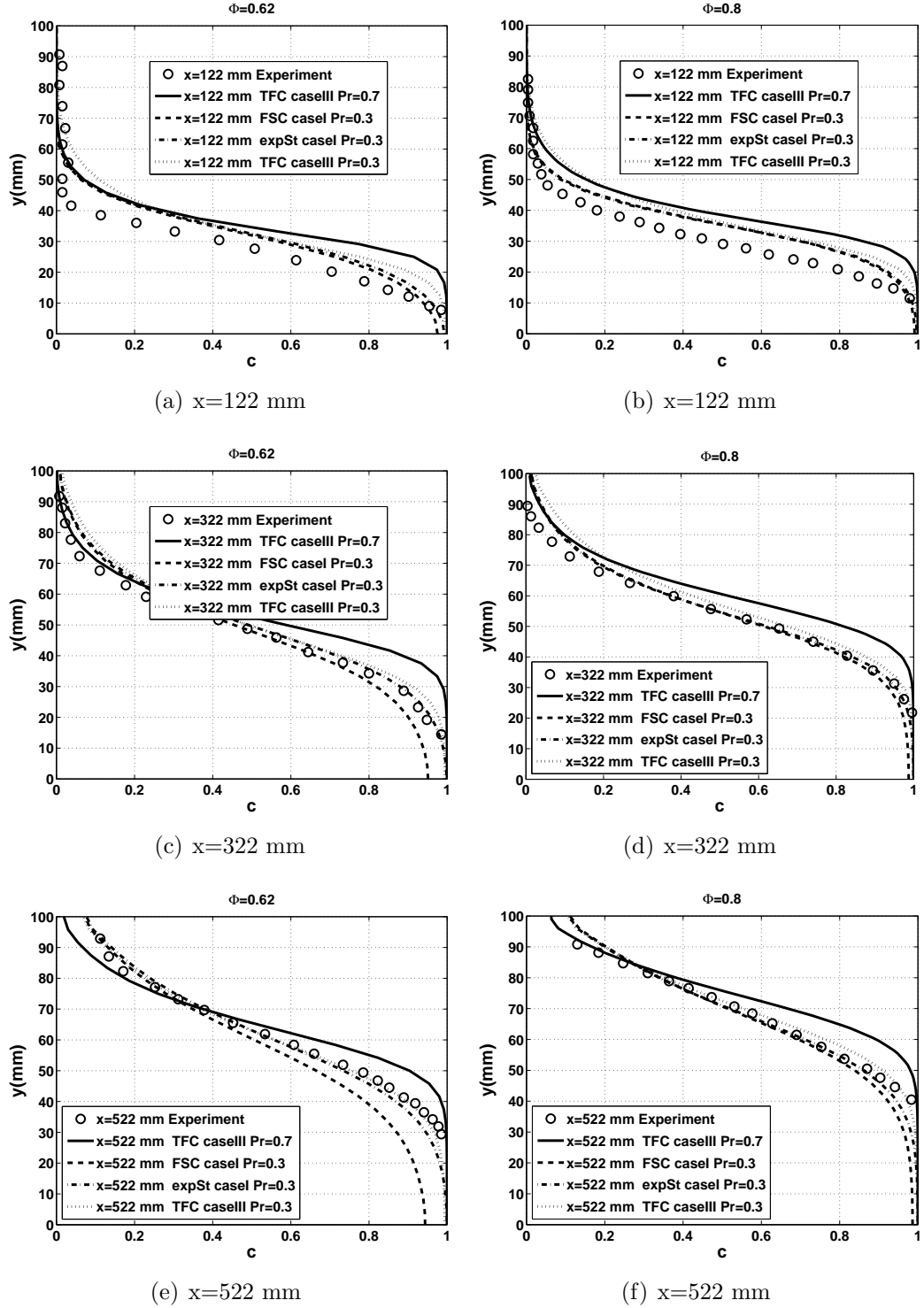


Figure 4.13: Simulated \tilde{c} profiles at different positions within the combustion chamber obtained using the TFC ($Pr=0.7$ and 0.3 , case III dissipation rate), FSC, and FSC+exp source term models ($Pr=0.3$, case I dissipation rate) at $\Phi = 0.62$ and 0.80

4.2. HIGHLY TURBULENT CONFINED FLAMES

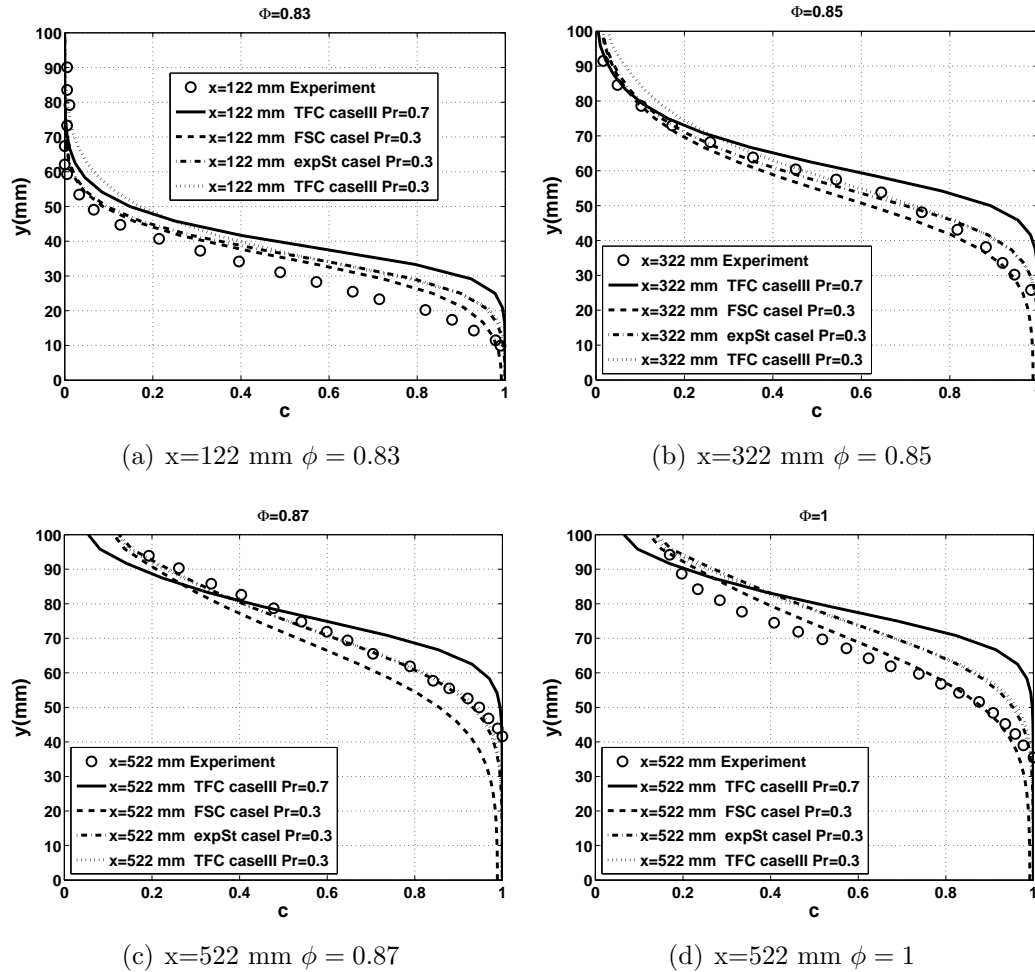


Figure 4.14: Comparison between TFC ($\text{Pr}=0.7, 0.3$, caseIII), FSC and FSC+exp source term ($\text{Pr}=0.3$, caseI) at $\Phi = 0.83, 0.85, 0.87, 1$

CHAPTER 4. MODEL VALIDATION

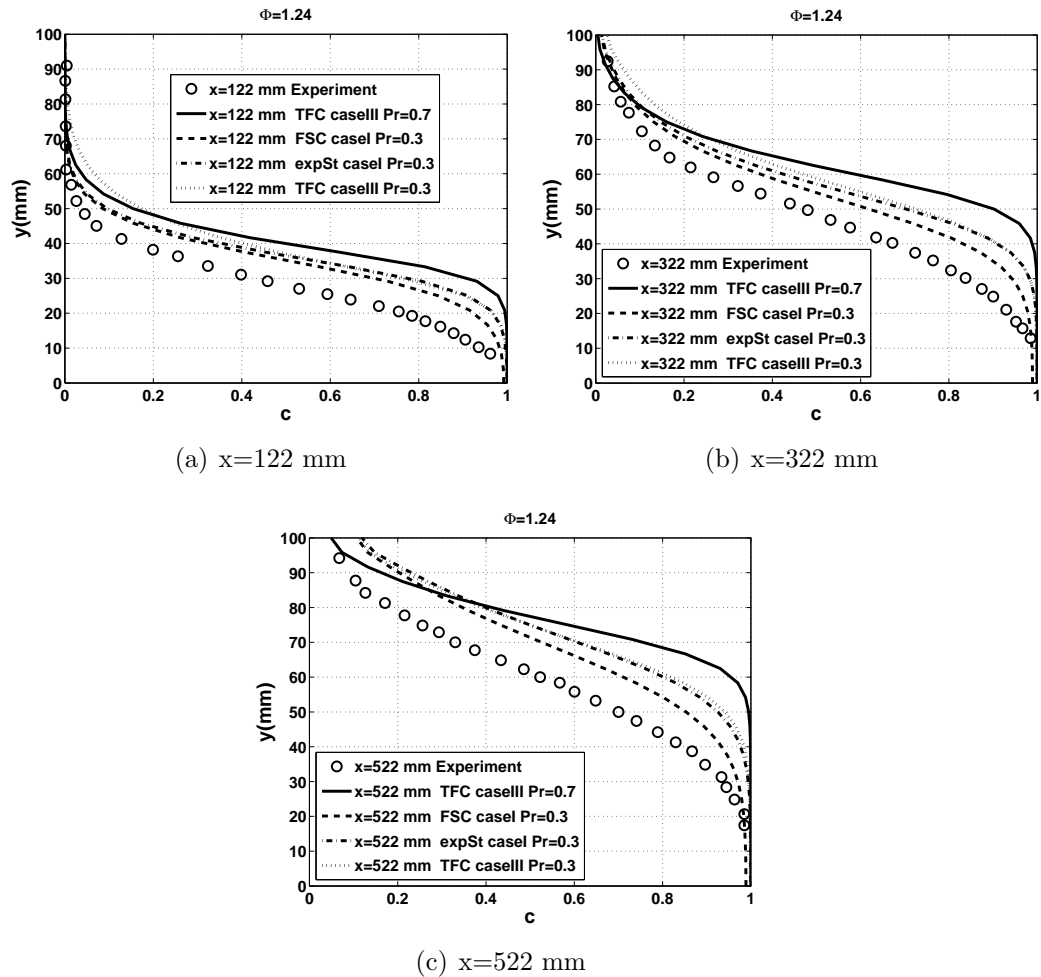


Figure 4.15: Comparison between TFC ($\text{Pr}=0.7, 0.3$, caseIII), FSC and FSC+exp source term ($\text{Pr}=0.3$, caseI) at $\Phi = 1.24$

4.2.4 Conclusion

The TFC and FSC models of premixed turbulent combustion were implemented in OpenFOAM and used to simulate the experiments reported by Moreau [1], who studied oblique preheated lean methane-air flames generated from mixtures with different equivalence ratios ($\Phi=0.62\text{-}1.24$) in a highly intense turbulent flow with stabilization by a hot product flow in an adjacent channel. The values of two parameters used in these models - the dissipation rate and the turbulent Prandtl number - were tuned to reproduce the experimental results for a single equivalence ratio ($\Phi = 0.8$). The resulting tuned values were then used without further modification to simulate the experiments performed at other equivalence ratios. Comparison of results computed using the two models, with all other things being equal, indicates that premixed turbulent flame development plays a role by reducing the burning rate and mean flame brush thickness in the considered case. The reasonable agreement between the experimental and numerical data shows that both models are capable of reproducing experimental results with at least some level of accuracy but cannot be taken as a complete validation of their predictive capabilities because the results obtained were sensitive to the inflow boundary condition for the mean dissipation rate. However, this sensitivity was less pronounced for the FSC model.

4.3 V-shape flames

4.3.1 The simulated test case

The second experimental study that was used as a source of reference data in this work was the examination of non-confined turbulent premixed V-shaped flames conducted by Dinkelacker and Hölzler [2]. Figure 4.16(a) shows the experimental setup used by these authors. Their apparatus features a nozzle with a diameter of 40 mm and a perforated plate that is located 70 mm beneath the nozzle's aperture. In addition, there is a 2 mm stabilizer wire located 10 mm above the nozzle exit. These experiments are attractive as sources of reference data for numerical simulations because of the simple geometric configuration of the flow and the homogeneous turbulence created by using a perforated plate. Moreover, the mean flame location in this system can be specified in terms of the flame angle, which is a useful parameter when comparing simulated and experimental data. Several groups have therefore conducted modeling studies based on these experiments:

- i) Dinkelacker and Hölzler [2] conducted studies using the TFC model and two other models with different expressions for the reaction rate
- ii) Ghirelli [37] performed investigations using the original TFC model and a modified variant that is based on Ghirelli's dispersion model [38].
- iii) Moreau [46] [47] studied the Dinkelacker and Hölzler system using the original TFC model and a modified variant known as the self-similar turbulent flame (SSTF) model

However, the FSC model has not yet been used to simulate these experiments.

4.3.2 Numerical setup and sensitivity analysis

Simulations were performed for all three of the equivalence ratios examined by Dinkelacker and Hölzler ($\Phi = 0.5$, $\Phi = 0.58$, $\Phi = 0.7$) and with the mean inlet velocity equal to 3.04 m/s. Simulations performed using the TFC (equations 2.24 and 2.26) and FSC (equations 2.30 2.28 and 2.29) models. The standard $k-\varepsilon$ model [39] was used to simulate the turbulence in each case. Two additional sets of simulations were conducted to investigate the effect of compressibility in this system, since it is known to be important in engines. The first set was conducted using the FSC model with the standard $k-\varepsilon$ model ($c_3 = 0$), while the second set used the FSC model in conjunction with the extended $k-\varepsilon$ model ($c_3 = -0.33$, see equation 2.36). The progress variable fields for these two cases are shown in figure 4.17

4.3. V-SHAPE FLAMES

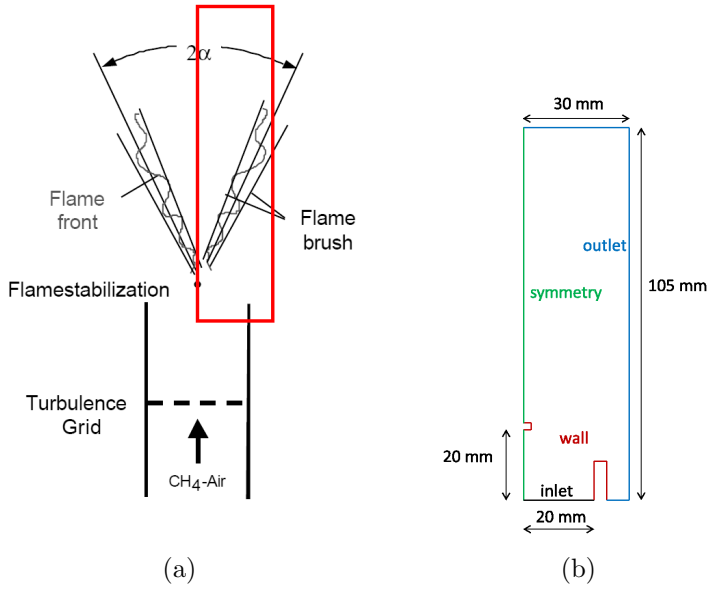


Figure 4.16: a) The experimental setup used by Dinkelacker and Hölzler to study V-shaped flames [2] b) The dimensions of the simulated combustion chamber used in the numerical studies based on the Dinkelacker and Hölzler experiments

for different equivalence ratios; this figure clearly indicates that compressibility has negligible effects in this experiment. Therefore, all subsequent simulations were conducted using the standard $k-\epsilon(c_3 = 0)$ model.

While the experiments examined by Dinkelacker and Hölzler [2] was not two dimensional, the system has no significant three dimensional effects as investigated by the authors [2] and so two-dimensional simulations were performed to minimize the computational cost of the study. In addition, due to the symmetric nature of the v-shaped flames investigated, only half of the flow was simulated directly (this part of the flow is indicated by the red rectangle in figure 4.16(a)), using a symmetry boundary condition. Preliminary investigations were also conducted using 2D axisymmetric simulations, but these did not yield promising results and so this approach was abandoned. The upper outlet boundary is located 85 mm above the wire, and the outlet boundary on the right hand side is 30 mm from the center line as shown in figure 4.16(a). The simulated test case is shown in figure 4.16(b).

Unsteady simulations were allowed to proceed until a stationary solution was obtained. Figure 4.18 shows the development of the simulated flame along the y direction in a typical case.

Preliminary simulations were conducted to establish the mesh independence of the simulated system; based on the results obtained, grids with 15760 cells were used in all subsequent simulations. Simulations with larger

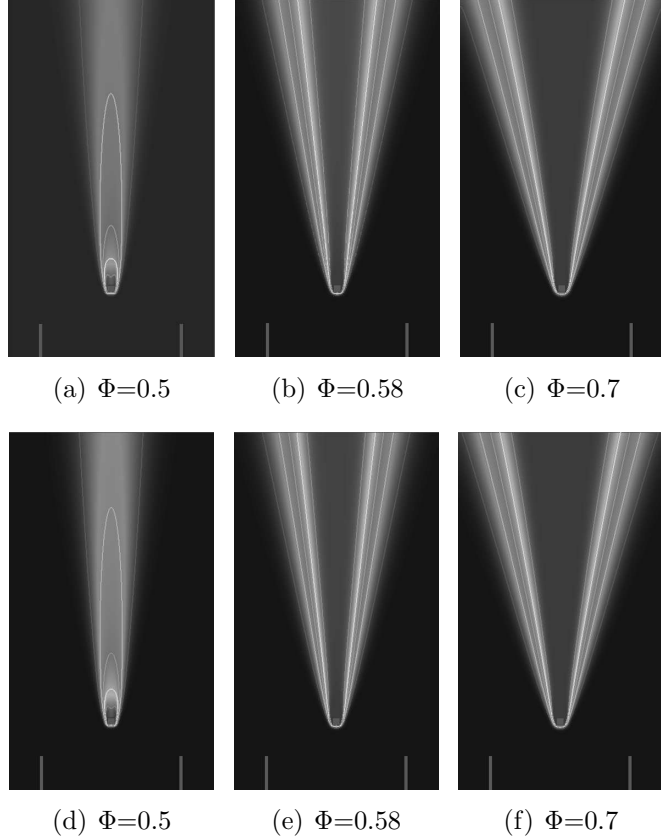


Figure 4.17: \bar{c} field for the FSC model at different equivalence ratios and $\varepsilon = 0.96 \text{ m}^2/\text{s}^3$ with $Pr = 0.3$, $c_3 = 0$ (a, b, c) and $c_3 = -0.33$ (d, e, f)

domains were also conducted to assess the sensitivity of the results to the domain size. In section 4.3.3, it is shown that the flame takes a curved shape in the richest of the studied cases ($\Phi = 0.7$) and extends all the way to the right-hand side boundary of the simulated system. To determine whether this flame shape was affected by the size of the simulated domain, a simulation was performed using the TFC model under the assumption that $Pr_t = 0.7$ with a larger domain. The results are shown in figure 4.19, which clearly indicates that the domain size did not significantly affect the results obtained: the half-flame angles in the small- and large-domain cases are almost identical. The smaller domain size was therefore used in all subsequent simulations. It should be noted that it was essential to have good starting conditions in order to achieve convergence when using the larger domain whereas the smaller domain was less sensitive.

Even when using the smaller domain, it was necessary to perform an initial simulation with a cold flow and use the resulting converged results

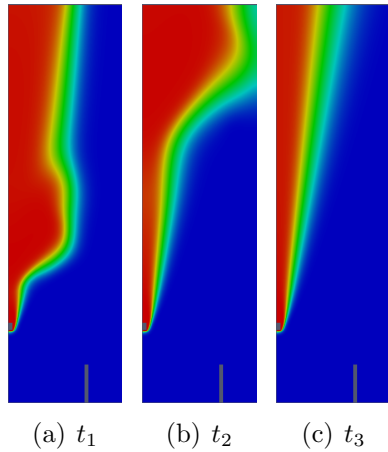


Figure 4.18: Development of the V-shaped flames over time

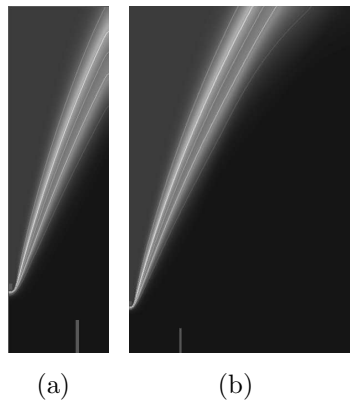
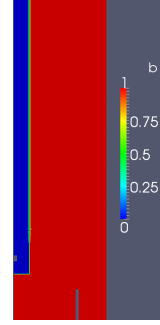


Figure 4.19: Comparison of the \bar{c} fields for small (a) and large (b) domains

as a starting point for the hot flow simulation in order to obtain a faster converged solution. Figure 4.20 shows the initial conditions imposed in terms of the value taken by the regress variable, \tilde{b} , which is defined as $\tilde{b} = 1 - \tilde{c}$. The area inside the red rectangle is assumed to be filled with burned products and therefore $\tilde{b} = 0$. A similar initial condition was imposed on the density field. This was found to facilitate and expedite convergence.

The boundary conditions imposed in the V-shaped flame simulations are specified in figure 4.16(b). The inlet flow was subject to a boundary condition that was defined by the values specified in table 4.4 and 4.5, which were chosen based on experimental data [2]. Table 4.4 lists the values for several key parameters in the v-shaped flame simulations, including the mean flow velocity, U , velocity fluctuations, u'_x , u'_y , length scale, L , kinetic

Figure 4.20: Initial condition for $\tilde{b} = 1 - \tilde{c}$ value

$U(m/s)$	$u'_x(m/s)$	$u'_y(m/s)$	$L(mm)$	$k(m^2/s^2)$	$\varepsilon(m^2/s^3)$
3.08	0.29	0.24	5.4	0.1	$\varepsilon(C_D)$

Table 4.4: Inflow boundary conditions for the v-shaped flame simulations

energy, $k = 0.5(u'_x^2 + 2u'_y^2)$, and dissipation rate, ε . In addition, the value of the Favre-averaged progress variable was set to zero at the stabilizer wire and a symmetry boundary condition was imposed at the symmetry line. Wall functions and outflow boundary conditions were imposed at the other boundaries of the simulated domain.

The values taken by other parameters, including the burned temperature, T_b , density, ρ , viscosity, ν , thermal diffusivity, κ , laminar flame speed, S_L and time, t_r are presented in table 4.5. These values were computed using the PREMIX code [40] of the CHEMKIN package [42] in conjunction with the GRI 3.0 chemical mechanism [41].

Φ	0.5	0.58	0.7
$T_b[K]$	1480	1628	1840
$\rho_u[kg/m^3]$	1.135	1.131	1.125
$\rho_b[kg/m^3]$	0.230	0.208	0.1838
$\nu_u[m^2/s]$	1.58e-5	1.59e-5	1.59e-5
$\nu_b[m^2/s]$	2.378e-4	2.798e-4	3.416e-4
$\kappa_u[m^2/s]$	2.24e-5	2.24e-5	2.24e-5
$\kappa_b[m^2/s]$	4.84e-4	3.95e-4	3.36e-4
$S_L[m/s]$	0.048	0.104	0.196
$t_r[s]$	9.96e-10	6.23e-10	9.8e-10

Table 4.5: Values taken by selected parameters in the v-shaped flame simulations

4.3.3 Results, validation, and discussion

This section presents the results obtained in the V-shaped flame simulations. It is subdivided into sections discussing the following topics

- i) The effects of varying the Pr_t number
- ii) The effects of varying the dissipation rate
- iii) Validation of the tested models

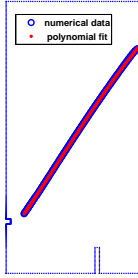


Figure 4.21: 4^{th} order polynomial fit for the \bar{c} iso-line

As discussed in section 2.8, it was necessary to tune the values of both the Pr_t number and the dissipation rate in order to obtain reasonable results in the simulations. The results of tuning of these two parameters are discussed in subsections i and ii, respectively. In brief, the tuning process involved conducting a series of simulations for a single experimental case ($\Phi = 0.7$) and varying the value of the parameter to be tuned in order to identify that which gave the best agreement with the experimental data. The tuned value obtained in this way was then used in simulations of different experimental cases (i.e. simulations of flames generated at different equivalence ratios). The final subsection discusses the results obtained using the tuned parameter values and the different tested models in terms of the \bar{c} field and the flame half angle, and compares the simulated results to the experimental data.

The flame half-angle was computed by post-processing the iso-lines of the \bar{c} field for $\bar{c} = 0.5$. The \bar{c} field was calculated using equation 2.20. The Matlab post-processing code was then used to fit a 4^{th} order polynomial over the $\bar{c} = 0.5$ isoline and the flame half-angle was calculated as the derivative of the resulting curve at distances of 15 mm, 30 mm, and 45 mm away from the flame holder in the y direction. Figure 4.21 shows that this 4^{th} order polynomial provides a very good approximation of the \bar{c} iso-line. It worth mentioning that 3^{rd} order and higher-order polynomial were also

CHAPTER 4. MODEL VALIDATION

tested and yielded very similar flame angles to those obtained using the 4th order polynomials.

The results are presented in the following order:

- The effects of varying the Pr_t number
 - 1. In FSC simulations assuming $\varepsilon = 0.96 \text{ m}^2/\text{s}^3$
 - 2. In FSC simulations using an exponential source term and assuming that $\varepsilon = 0.96$ or $4.80 \text{ m}^2/\text{s}^3$
- The effects of varying the dissipation rate
 - 3. In TFC simulations assuming $Pr_t = 0.7$, $\Phi = 0.7$
 - 4. In FSC simulations using an exponential source term and assuming that $Pr_t = 0.5$
- Validation and Comparison

4.3. V-SHAPE FLAMES

- The effects of varying the Pr_t number in FSC simulations assuming $\varepsilon = 0.96 \text{ m}^2/\text{s}^3$

FSC simulations were conducted using Pr_t values of 0.3 and 0.7 in order to determine how varying the Prandtl number affected the predicted burning rate and flame brush thickness. In all cases, it was assumed that $\varepsilon = 0.96 \text{ m}^2/\text{s}^3$. The \bar{c} fields obtained using these two values of Pr_t at different equivalence ratios are shown in figure 4.22. Increasing the Pr_t number from 0.3 to 0.7 decreases the fully turbulent diffusivity according to equation 2.25 but increases the magnitude of the time-dependent term in equation 2.28 because it decreases the Lagrangian time scale, $\tau_L = D_{t,\infty}/S_L^2$. The net effect of increasing Pr_t is thus to decrease the time-dependent diffusivity, $D_{t,t}$ and hence the flame brush thickness. This effect was observed at all of the studied equivalence ratios, and is summarized in equation 4.5. It should be noted that changes in the Pr_t number also have minor effects on the kinetic energy, k , turbulent time scale τ_t and length scale, L .

$$Pr_t \uparrow \implies D_{t,\infty} \downarrow \implies \tau_L \downarrow \implies D_{t,t} \downarrow \implies \text{Thickness} \downarrow \quad (4.5)$$

The turbulent burning rate is also affected by changes in the value of the Pr_t number. τ_L decreases when the Pr_t number increases because this reduces the magnitude of $D_{t,\infty}$. Decreases in τ_L increase the value of the time-dependent term of equation 2.29, causing the burning rate to increase. This in turn causes the flame half-angle and flame width to increase. These effects are summarized in equation 4.6.

$$Pr_t \uparrow \implies D_{t,\infty} \downarrow \implies \tau_L \downarrow \implies \text{Burning rate} \uparrow \quad (4.6)$$

The FSC model was not capable of reproducing the properties of the experimental flame when using a Pr_t value of 0.3 due to the low burning rate obtained under these conditions. However, as the equivalence ratio was increased, the laminar flame speed rose from 0.048 m/s to 0.196 m/s and so the chemical time scale decreased ($\tau_c = \kappa_u/S_L^2$). This caused an increase the value of the Da number, τ_t/τ_c and therefore increased the fully developed turbulent burning velocity according to equation 2.26. Therefore, at higher equivalence ratios, the properties of the experimental flame are reproduced and the simulated flame width increases as shown in figure 4.22 (a, b, c). Equation 4.7 summarizes this trend.

$$\Phi \uparrow \implies S_L \uparrow \implies \tau_c \downarrow \implies Da \uparrow \implies U_t(\text{Burning rate}) \uparrow \quad (4.7)$$

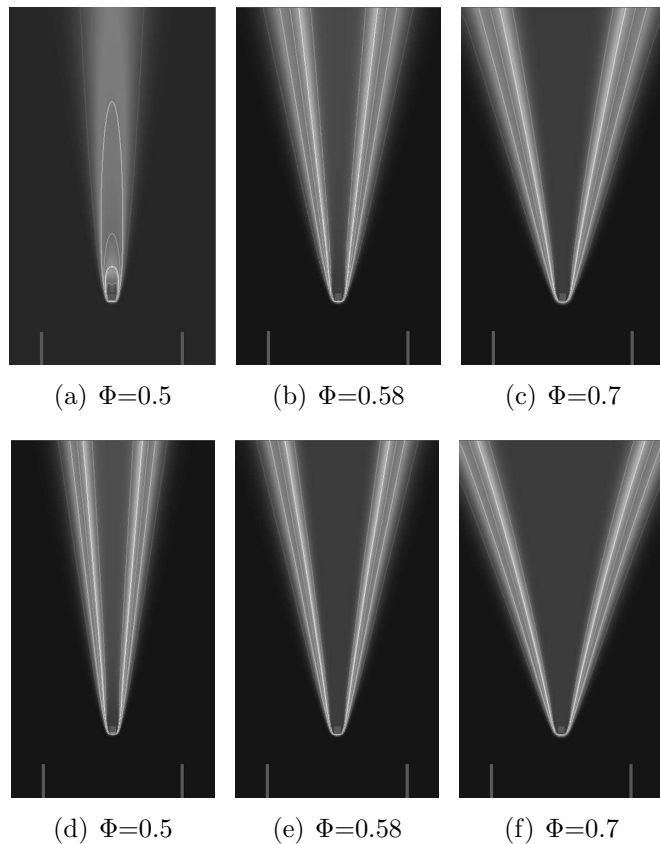


Figure 4.22: The effect of varying the Pr_t number on the \bar{c} field predicted using the FSC model at different equivalence ratios, assuming that $\varepsilon = 0.96 \text{ m}^2/\text{s}^3$ (figures a, b, and c show fields for $Pr_t = 0.3$; figures d, e, and f show fields for $Pr_t = 0.7$)

4.3. V-SHAPE FLAMES

The increases in the burning rate caused by increasing the Pr_t number or the equivalence ratio are also readily apparent in figure 4.23, which shows plots of the flame half-angle against Φ for two different Pr_t numbers.

In the leanest case for which experimental data are available ($\Phi = 0.7$), the simulations accurately reproduced the experimental results using a Pr_t number of 0.7. However, to identify an optimal value of Pr_t for general use, additional simulations were conducted.

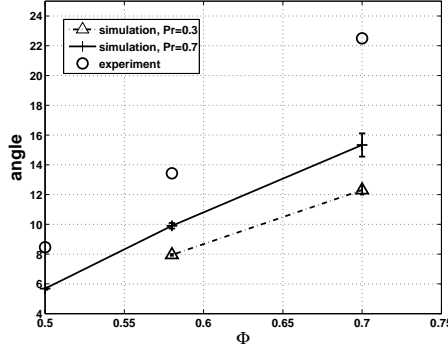


Figure 4.23: The flame half-angle as a function of Φ for $Pr_t = 0.3$ and $Pr_t = 0.7$ as predicted using the FSC model with $\varepsilon = 0.96 \text{ m}^2/\text{s}^3$

The simulated results shown in figure 4.23 indicate that the FSC model underestimates the measured burning rate if the exponential source term is omitted. As shown in the next subsection, the inclusion of this source term can be quite important when considering the weakly turbulent conditions associated with the studied flames.

- The effects of varying the Pr_t number in FSC simulations using an exponential source term and assuming $\varepsilon = 0.96 \text{ m}^2/\text{s}^3$, $\Phi = 0.7$

Simulations were performed using the FSC model with an exponential source term for five different Pr_t numbers (ranging from 0.3 to 0.7) at a single equivalence ratio, $\Phi = 0.7$, in order to identify the value that would yield the closest agreement with the experimental data. The effects of varying the Pr_t number on the simulated flame brush thickness and turbulent burning rate were similar to those discussed in the previous subsection and summarized in equations 4.6 and 4.5.

Figure 4.22 clearly shows that the inclusion of an extra source term in the equation for \tilde{c} in these simulations produces a thinner predicted flame brush than was obtained in its absence.

Variation of the Pr_t number can also affect the turbulent burning rate. As can be seen in figure 4.24, the turbulent burning rate increases in parallel with Pr_t . That is to say, the flame width and the flame half-angle are

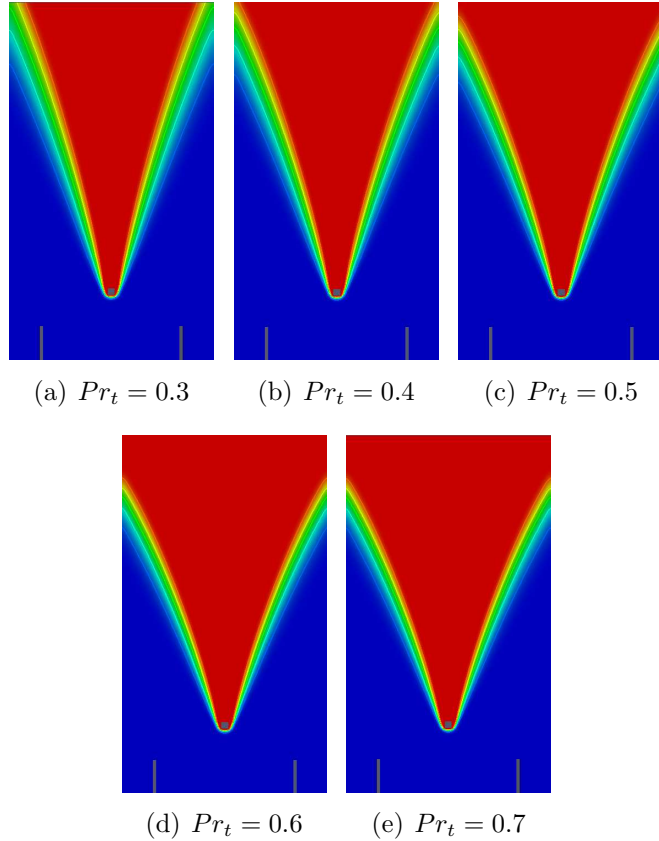


Figure 4.24: The effects of varying the Pr_t number on the \bar{c} fields obtained in FSC simulations using an exponential source term at $\Phi = 0.7$ and $\varepsilon = 0.96 \text{ m}^2/\text{s}^3$

increased by increasing the value of Pr_t . This trend is more apparent in figure 4.25, which shows that the flame half-angle at $\bar{c} = 0.5$ increases as the Pr_t number is increased. This occurs because increasing the Pr_t number decreases the value of τ_L as a consequence of a reduction in the fully developed turbulent diffusivity according to equation 2.25. This in turn increases the magnitude of the time-dependent term in equation 2.29, which corresponds to an increase in the burning rate. These trends are summarized in equation 4.6.

As can be seen in figure 4.25, larger values of the Pr_t number yield flame half-angles that more closely match the experimental data. However, they are also associated with larger error bars and a stronger flame curvature as shown in figure 4.24. A Pr_t value of 0.5 was therefore identified as being optimal since it gives reasonably good agreement with the experimental data without producing excessively large error bars and is also relatively close to the tuned value used to simulate the Moreau experiments ($Pr_t = 0.3$) as

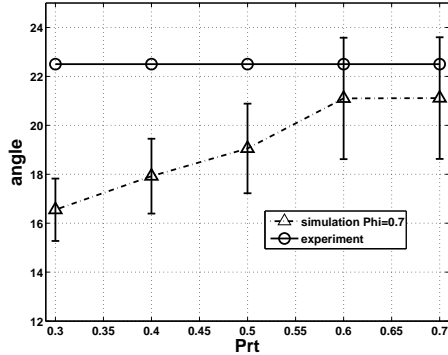


Figure 4.25: Variation in the flame half angle for different Pr_t numbers as predicted using the FSC model with an exponential source term, assuming $\varepsilon = 0.96 \text{ m}^2/\text{s}^3$

discussed in the preceding section of the results. The agreement between the experimental and simulated results can be further improved by changing the value of the constant C_D in equation 2.39 as discussed in the following subsections.

- The effect of varying the dissipation rate in TFC simulations assuming $Pr_t = 0.7$, $\Phi = 0.7$

Dinkelacker and Hözlér presented the integral length scales when analyzing their experimental work [2]. However, as discussed in section 2.8, the C_D term in equation 2.39 is a function of the Reynolds number and therefore requires tuning. To identify the optimal value of this parameter, we performed calculations using four different C_D values (0.15, 0.3, 0.9, and 1.5), with four different associated inlet dissipation rates as described by equation 2.39. The length scale at the inlet boundary was kept constant in all cases and took the value specified in table 4.4. The Pr_t number was set to 0.7 and the equivalence ratio was set to $\Phi = 0.7$, corresponding to the richest case examined by Dinkelacker and Hözlér in their experimental work. The simulations were performed using the TFC model in order to investigate the effect of varying the dissipation rate and to identify the dissipation rate that would yield the closest agreement with the experimental data. The \bar{c} fields obtained in each case are shown in figure 4.26.

Increasing the dissipation rate at the boundary decreases the turbulent diffusivity according to equation 2.25. This reduces the flame brush thickness, as can be seen in figure 4.26.

Figure 4.27 indicates a weak influence of the inlet dissipation rate (or C_D) on the computed flame half-angle. Because previous studies in this area have used a value of $C_D = 0.3$, which corresponds to $\varepsilon = 0.96 \text{ m}^2/\text{s}^3$, the latter value was used in subsequent simulations using the TFC model.

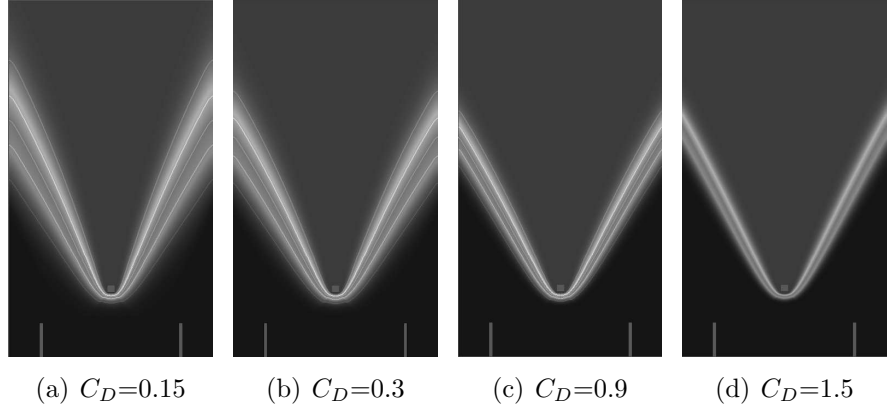


Figure 4.26: \bar{c} fields obtained using the TFC model at $\Phi=0.7$ and $A=0.50$ for different dissipation rates

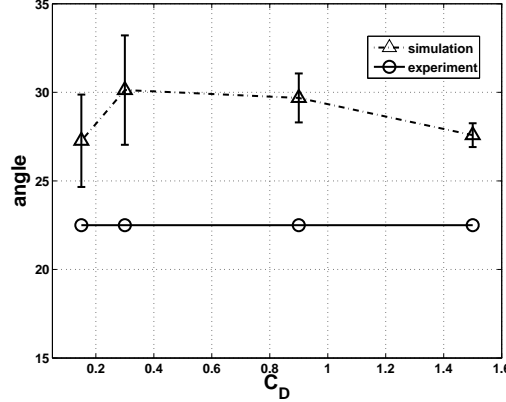


Figure 4.27: Plots of the flame half-angle against C_D based on TFC simulations with $Pr_t = 0.7$, at $\Phi = 0.7$

- The effect of varying the dissipation rate in FSC simulations using an exponential source term and assuming $Pr_t = 0.5$

FSC simulations with an exponential source term were performed using four different dissipation rates that were selected based on four different values of the constant C_D . The Pr_t value was set to 0.3 and the value of the c_3 in the $k - \varepsilon$ model was set to 0. The effects of varying the dissipation rate on the outcomes of these simulations are shown in figures 4.28 and 4.29.

Increasing the dissipation rate decreases both $D_{t,\infty}$ and τ_L which in total leads to a decrease in time dependent turbulent diffusion. Consequently turbulent flame brush thickness reduces as shown in figure 4.28.

Increases in the dissipation rate decrease $D_{t,\infty}$ and therefore τ_L . Consequently, the time-dependent term in equation 2.29 will increase, causing an

4.3. V-SHAPE FLAMES

increase in the burning rate. This is reflected in figures 4.28 and 4.29, which show that the flame width and flame half-angle increase as the dissipation rate is increased.

$$\boxed{\varepsilon \uparrow \implies D_{t,\infty} \downarrow \implies \tau_L \implies \text{Thickness} \downarrow} \quad (4.8)$$

$$\boxed{\varepsilon \uparrow \implies D_{t,\infty} \downarrow \implies \tau_L \downarrow \implies \text{Burning rate} \uparrow} \quad (4.9)$$

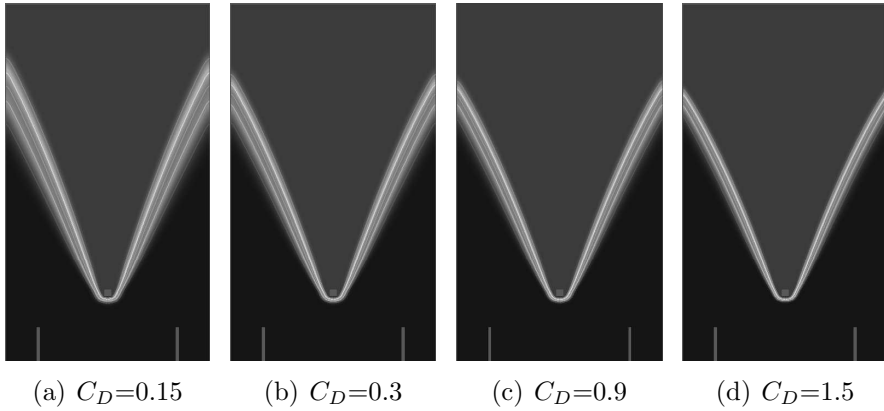


Figure 4.28: \bar{c} field obtained using the FSC model with an exponential source term at $\Phi = 0.7$ at $Pr_t = 0.5$

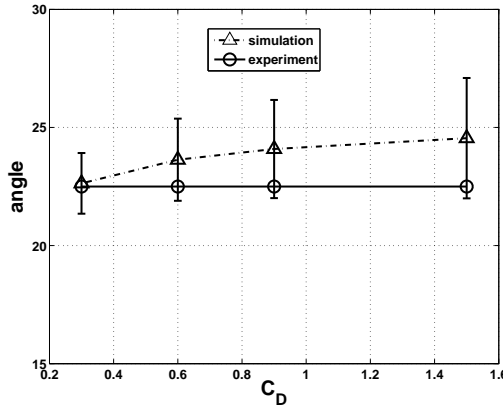


Figure 4.29: The flame half angle obtained using the FSC model with an exponential source term, shown as a function of the C_D rate for the case where $Pr_t = 0.3$ and $\Phi = 0.7$

- Validation and Comparison:

The preceding subsections describe the tuning of two parameters used in the studied models - the inlet dissipation rate (or C_D) and the Pr_t number - in order to reproduce the experimental results of Dinkelacker and Hölzler for the $\Phi = 0.7$ case. For the TFC model, it was found that the computed burning rate was weakly sensitive to Pr_t and C_D . Accordingly, in order to be consistent with previous studies in this area, a Pr_t value of 0.7 and a C_D value of 0.3 (which corresponds to $\varepsilon = 0.96 \text{ m}^2/\text{s}^3$) were selected for use in subsequent simulations.

For the FSC model with an exponential source term, it was found that increasing the value of the Pr_t number increased the computed burning rate and a Pr_t value of 0.5 was selected. This value was used in FSC simulations performed with and without an exponential source term. Although a C_D value of 0.3 gave the best agreement with the measured flame half-angle, a larger C_D value of 0.9 was used in all subsequent FSC simulations in order to be consistent with an increase in C_D with decreasing Reynolds number, see figure 2.2.

Figures 4.30-4.32 summarize the results obtained in the simulations of the Dinkelacker and Hölzler experiments conducted using the TFC and FSC models and with the FSC model with an exponential source term. Figure 4.32 shows that the FSC model with an exponential source term well predicts the measured flame half-angle for all three equivalence ratios, whereas the TFC model slightly overpredicts the burning rate. Comparison of computed flame images (figure 4.30) with measured ones (figure 4.31) implies that the TFC model predicts the mean flame brush thickness in the richest case better than the FSC model does, but the lack of quantitative data on the mean flame brush thickness in the paper by Dinkelacker and Hölzler [2] does not allow us to draw more solid conclusions.

All in all, both the TFC and FSC models perform reasonably well in the studied case.

The large values of C_D used in these investigations are consistent with the available DNS data, which indicate that C_D increases significantly as Re_t decreases in weakly turbulent flows. This is shown in figure 2.2.

4.3. V-SHAPE FLAMES

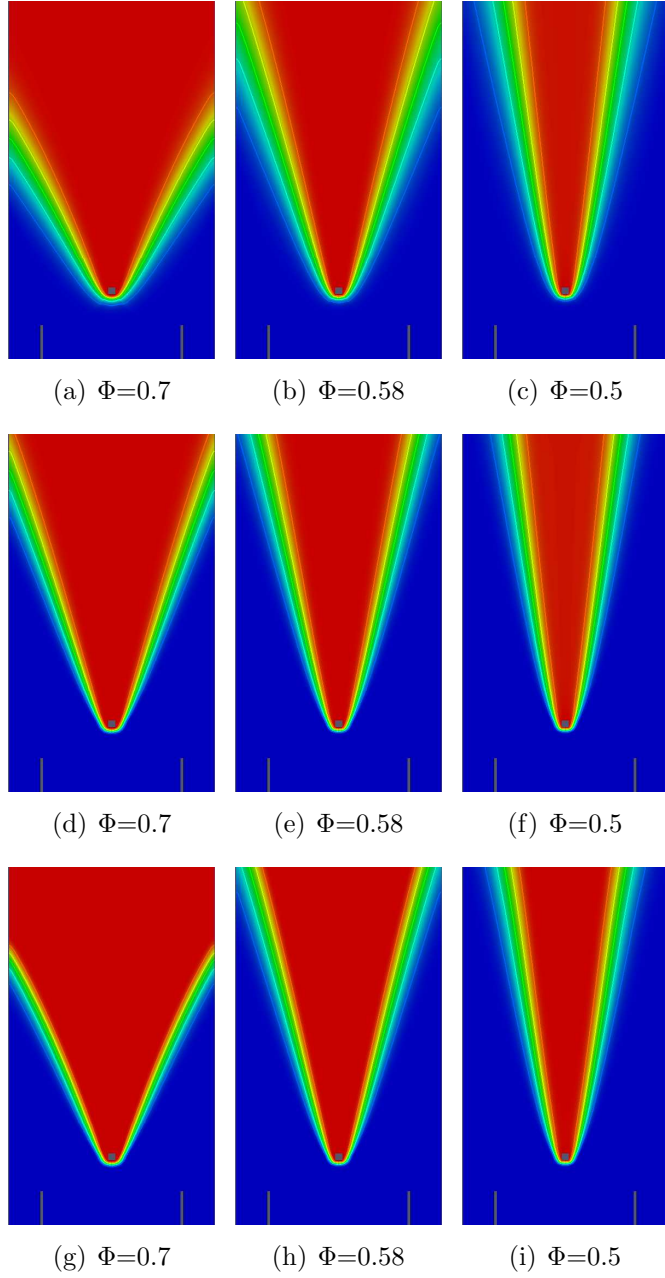


Figure 4.30: \bar{c} fields obtained in simulations of the V-shaped flames formed at different equivalence ratios using different models. The top, middle, and bottom rows show the results obtained using the TFC model (assuming that $Pr_t = 0.7$ and $\varepsilon = 0.96 \text{ m}^2/\text{s}^3$), the FSC model, and the FSC model with an exponential source term, respectively. In all simulations using the FSC model, it was assumed that $Pr_t = 0.5$ and $\varepsilon = 2.88 \text{ m}^2/\text{s}^3$.

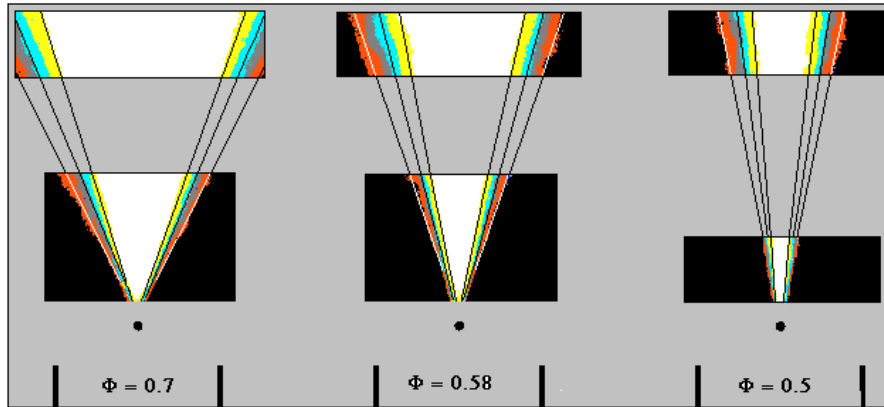


Figure 4.31: \bar{c} fields observed by Dinkelacker and Hözlér [2] at different equivalence ratios in their experimental studies

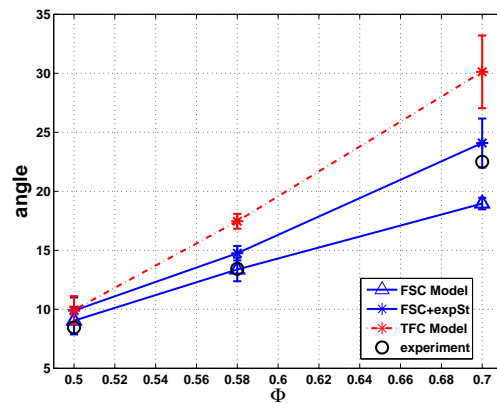


Figure 4.32: Plots of the simulated flame half-angle against the equivalence ratio for the TFC ($Pr_t = 0.7$, $\varepsilon = 0.96$), FSC, and FSC with an exponential source term ($Pr_t = 0.5$, $\varepsilon = 2.88$) models

Chapter 5

Concluding remarks and future work

The OpenFOAM library was extended to simulate premixed turbulent combustion within the framework of the RANS paradigm. In particular, the original library was found to yield an incorrect mean density for the reacting mixture and so a proper method for evaluating the mean density based on the well-known equation 2.19 was implemented into the code. In addition, two well-known models (TFC and FSC) for describing the influence of turbulence on premixed combustion were also implemented into OpenFOAM.

The so-extended code was successfully applied to simulate two widely recognized sets of experiments with two substantially different, well-defined, simple, laboratory premixed turbulent flames, i.e. (i) the oblique, confined, preheated, highly turbulent methane-air flames experimentally studied by Moreau [1] and (ii) the V-shaped, open, weakly turbulent, lean methane-air flames investigated by Dinkelacker and Hölzler [2] under the room conditions. In both sets of measurements, burning with different equivalence ratios was studied.

The computed results agree both qualitatively and quantitatively with the aforementioned experimental data, thus, validating both the implemented combustion models and the extended code. A comparison of the results computed using the TFC and FSC models, with all other things being equal, indicates that an early stage of premixed turbulent flame development, which is solely addressed by the latter model, plays a role by reducing the burning rate and mean flame brush thickness in the considered cases.

It is worth stressing that the single constant A of the TFC and FSC models was not tuned in the present study, i.e. the same value of $A = 0.5$ that is recommended in the literature was used in all of the simulations discussed herein. However, in order to obtain the quantitative agreement with

CHAPTER 5. CONCLUDING REMARKS AND FUTURE WORK

the experimental results, two input parameters of the turbulence model, i.e. (i) the inlet dissipation rate and (ii) the turbulent Prandtl number, required tuning, because the available data on these two quantities are controversial. In the present work, these two input parameters were tuned for a single reference case for each set of experiments and the same values were used to simulate all other cases experimentally investigated either by Moreau [1] or by Dinkelacker and Hölzler [2]. Therefore, these simulations showed that both models were capable of accurately and quantitatively predicting the effects of variation in the equivalence ratio without requiring further tuning.

According to the schedule of the present project, the main focus of future work will be placed on (i) further extension of OpenFOAM library in order to simulate turbulent scalar flux invoking recent advanced models for conditioned velocities in premixed turbulent flames and (ii) application of the so-extended code to multi-dimensional unsteady RANS simulations of turbulent combustion in Direct Injection Stratified Charge Spark Ignition engines. The demonstrated ability of the TFC and FSC models to well predict turbulent burning rates for various equivalence ratios makes these two models particularly interesting for the latter purpose.

References

- [1] P. Moreau, “Turbulent flame development in a high velocity premixed flow,” in *American Institute of Aeronautics and Astronautics, Aerospace Sciences Meeting, 15 th, Los Angeles, Calif*, 1977.
- [2] F. Dinkelacker and S. Hölzler, “Investigation of a turbulent flame speed closure approach for premixed flame calculations,” *Combustion science and technology*, vol. 158, no. 1, pp. 321–340, 2000.
- [3] D. Spalding, “Mixing and chemical reaction in steady confined turbulent flames,” in *Symposium (International) on Combustion*, vol. 13, no. 1. Elsevier, 1971, pp. 649–657.
- [4] B. F. Magnussen and B. H. Hjertager, “On mathematical modeling of turbulent combustion with special emphasis on soot formation and combustion,” in *Symposium (International) on Combustion*, vol. 16, no. 1. Elsevier, 1977, pp. 719–729.
- [5] V. Zimont and A. Lipatnikov, “A numerical model of premixed turbulent combustion of gases,” *Chem. Phys. Reports*, vol. 14, no. 7, pp. 993–1025, 1995.
- [6] A. Lipatnikov and J. Chomiak, “Turbulent flame speed and thickness: phenomenology, evaluation, and application in multi-dimensional simulations,” *Progress in energy and combustion science*, vol. 28, no. 1, pp. 1–74, 2002.
- [7] P. Sathiah and A. Lipatnikov, “Effects of turbulent flame speed development and axial convective waves on oscillations of a long ducted flame,” *Combustion Science and Technology*, vol. 179, no. 7, pp. 1433–1449, 2007.
- [8] K. Bray and J. Moss, “A unified statistical model of the premixed turbulent flame,” *Acta Astronautica*, vol. 4, no. 3, pp. 291–319, 1977.
- [9] P. A. Libby and K. Bray, “Variable density effects in premixed turbulent flames,” *AIAA Journal*, vol. 15, no. 8, pp. 1186–1193, 1977.

REFERENCES

- [10] A. Prudnikov, “Combustion of homogeneous fuel-air mixtures in turbulent flows,” *Physical basis of processes in combustion chambers of airbreathing engines. Moscow: Mashinostroenie*, pp. 255–347, 1964.
- [11] A. Prudnikov, “Hydrodynamics equations in turbulent flames,” *Combustion in a turbulent flow. Moscow: Oborongiz, chapter 1*, pp. 7–29, 1960.
- [12] V. Zimont, “Theory of turbulent combustion of a homogeneous fuel mixture at high reynolds numbers,” *Combustion, explosion, and shock waves*, vol. 15, no. 3, pp. 305–311, 1979.
- [13] V. L. Zimont, F. Biagioli, and K. Syed, “Modelling turbulent premixed combustion in the intermediate steady propagation regime,” *Progress in Computational Fluid Dynamics, An International Journal*, vol. 1, no. 1, pp. 14–28, 2001.
- [14] V. L. Zimont and F. Biagioli, “Gradient, counter-gradient transport and their transition in turbulent premixed flames,” *Combustion Theory and Modelling*, vol. 6, no. 1, pp. 79–101, 2002.
- [15] A. Lipatnikov, “Burning rate in impinging jet flames,” *Journal of Combustion*, vol. 2011, 2011.
- [16] V. Sabelnikov and A. Lipatnikov, “Towards an extension of tfc model of premixed turbulent combustion,” *Flow, Turbulence and Combustion*, pp. 1–14, 2012.
- [17] A. Lipatnikov and J. Chomiak, “A simple model of unsteady turbulent flame propagation,” *SAE transactions*, vol. 106, no. 3, pp. 2441–2452, 1997.
- [18] A. Lipatnikov and J. Chomiak, “Transient and geometrical effects in expanding turbulent flames,” *Combustion science and technology*, vol. 154, no. 1, pp. 75–117, 2000.
- [19] I. Zeldovich, G. I. Barenblatt, V. Librovich, and G. Makhviladze, “Mathematical theory of combustion and explosions,” 1985.
- [20] E. Shchetinkov, “Physics of gas combustion,” 1965.
- [21] R. S. Brodkey, “Fluid motion and mixing,” *Mixing Theory and Practice*, vol. 1, pp. 7–110, 1966.
- [22] S. B. Pope, *Turbulent flows*. Cambridge university press, 2000.

- [23] R. N. Dahms, M. C. Drake, T. D. Fansler, T.-W. Kuo, and N. Peters, “Understanding ignition processes in spray-guided gasoline engines using high-speed imaging and the extended spark-ignition model sparkcimm. part a: Spark channel processes and the turbulent flame front propagation,” *Combustion and flame*, vol. 158, no. 11, pp. 2229–2244, 2011.
- [24] K. R. Sreenivasan, “An update on the energy dissipation rate in isotropic turbulence,” *Physics of Fluids*, vol. 10, p. 528, 1998.
- [25] P. Yeung, D. Donzis, and K. Sreenivasan, “High-reynolds-number simulation of turbulent mixing,” *Physics of Fluids*, vol. 17, p. 081703, 2005.
- [26] P. Yeung and S. Pope, “Lagrangian statistics from direct numerical simulations of isotropic turbulence,” *Journal of Fluid Mechanics*, vol. 207, no. 1, pp. 531–586, 1989.
- [27] P. Yeung, “Lagrangian investigations of turbulence,” *Annual review of fluid mechanics*, vol. 34, no. 1, pp. 115–142, 2002.
- [28] D. Spalding, “Concentration fluctuations in a round turbulent free jet,” *Chemical Engineering Science*, vol. 26, no. 1, pp. 95–107, 1971.
- [29] B. Launder, “Heat and mass transport,” in *Turbulence*. Springer, 1978, pp. 231–287.
- [30] A. Reynolds, “The prediction of turbulent prandtl and schmidt numbers,” *International Journal of Heat and Mass Transfer*, vol. 18, no. 9, pp. 1055–1069, 1975.
- [31] K. Koeltzsch, “The height dependence of the turbulent schmidt number within the boundary layer,” *Atmospheric Environment*, vol. 34, no. 7, pp. 1147–1151, 2000.
- [32] T. K. Flesch, J. H. Prueger, and J. L. Hatfield, “Turbulent schmidt number from a tracer experiment,” *Agricultural and Forest Meteorology*, vol. 111, no. 4, pp. 299–307, 2002.
- [33] R. Bilger, L. Saetran, and L. Krishnamoorthy, “Reaction in a scalar mixing layer,” *Journal of Fluid Mechanics*, vol. 233, pp. 211–242, 1991.
- [34] R. Borghi and P. Moreau, “Turbulent combustion in a premixed flow,” *Acta Astronautica*, vol. 4, no. 3, pp. 321–341, 1977.

REFERENCES

- [35] L. Maciocco and V. Zimont, “Test of the TFC Combustion Model on High Velocity Premixed CH₄-Air Combustion in a Channel,” in *Proc. 20th Annual Meeting of the Italian Section of the Combustion Institute “Frantic97”, Cagliari, Italy*, 1997, pp. X–2.1–2.4.
- [36] V. Zimont and V. Battaglia, “Joint rans/les approach to premixed flame modelling in the context of the tfc combustion model,” *Flow, turbulence and combustion*, vol. 77, no. 1-4, pp. 305–331, 2006.
- [37] F. Ghirelli, “Turbulent premixed flame model based on a recent dispersion model,” *Computers & Fluids*, vol. 44, no. 1, pp. 369–376, 2011.
- [38] F. Ghirelli, “Eulerian modeling of turbulent dispersion from a point source,” *Computers & Fluids*, vol. 38, no. 9, pp. 1795–1798, 2009.
- [39] B. Launder and D. Spalding, “Mathematical Models of Turbulence,” *Academic Press*, 1972.
- [40] R. J. Kee, J. F. Grcar, M. Smooke, and J. Miller, “Premix: a fortran program for modeling steady laminar one-dimensional premixed flames,” Tech. Rep., 1985.
- [41] G. Smith, M. Golden, M. Frenklach, N. Moriarty, B. Eiteneer, M. Goldenberg, C. Bowman, R. Hanson, S. Song, W. Gardiner, V. Lissianski, and Z. Qin, “http://www.me.berkeley.edu/gri_mech/.”
- [42] R. J. Kee, J. A. Miller, and T. H. Jefferson, *CHEMKIN: A general-purpose, problem-independent, transportable, FORTRAN chemical kinetics code package*. Sandia Laboratories, 1980.
- [43] B. Launder and B. Sharma, “Application of the energy-dissipation model of turbulence to the calculation of flow near a spinning disc,” *Letters Heat Mass Transfer*, vol. 1, pp. 131–137, 1974.
- [44] V. Yakhot, S. Orszag, S. Thangam, T. Gatski, and C. Speziale, “Development of turbulence models for shear flows by a double expansion technique,” *Physics of Fluids A: Fluid Dynamics*, vol. 4, p. 1510, 1992.
- [45] T.-H. Shih, W. Liou, A. Shabbir, Z. Yang, and J. Zhu, “A new k-epsilon eddy viscosity model for high reynolds number turbulent flows: Model development and validation,” *NASA STI/Recon Technical Report N*, vol. 95, p. 11442, 1994.
- [46] V. Moreau, “Progress in the self-similar turbulent flame premixed combustion model,” *Applied Mathematical Modelling*, vol. 34, no. 12, pp. 4074–4088, 2010.

REFERENCES

- [47] V. Moreau, “A self-similar premixed turbulent flame model,” *Applied Mathematical Modelling*, vol. 33, no. 2, pp. 835–851, 2009.